stonehart associates

DOE/NASA/0176-81/5
CR 165594

PREPARATION AND EVALUATION OF ADVANCED ELECTROCATALYSTS FOR PHOSPHORIC ACID FUEL CELLS

8TH QUARTERLY REPORT

Paul Stonehart, John Baris, John Hochmuth and Peter Pagliaro

October - December 1981

PREPARED FOR:

NATIONAL AERONAUTICS AND SPACE ADMINISTRATION
Lewis Research Center
Under Contract DEN-3-176
Prepared Under Interagency Agreement DEAI-03-80ET17088

FOR:

U. S. DEPARTMENT OF ENERGY
Energy Technology
Division of Fossil Fuel Utilization

17 Cottage Road, Madison, Connecticut 06443
Telephone Area Code 203 245-7507

1. Report No.	2. Government Accession No.	3. Recipient's Catalog No.
NASA CR 165594		

4. Title and Subtitle	5. Report Date
PREPARATION AND EVALUATION OF ADVANCED ELECTRO-CATALYSTS FOR PHOSPHORIC ACID FUEL CELLS	December 31, 1981
	6. Performing Organization Code
7. Author(s)	8. Performing Organization Report No.
Dr. Paul Stonehart John Baris, John Hochmuth and Peter Pagliaro	
9. Performing Organization Name and Address	10. Work Unit No.
STONEHART ASSOCIATES, INC. 17 Cottage Road - P. O. Box 1220 Madison, CT 06443	11. Contract or Grant No. DEN-3-176
	13. Type of Report and Period Covered Contractor Report
12. Sponsoring Agency Name and Address U.S. Department of Energy Energy Technology Division of Fossil Fuel Utilization	14. Sponsoring Agency Code DOE/NASA/0176-81/5

15. Supplementary Notes
8th Quarterly Report Mail Stop 49-5, NASA-Lewis Research Center
Project Manager: Dr. M. Lauver, 21000 Brookpark Road, Cleveland, Ohio 44135
Prepared Under Interagency Agreement DEAI-03-80ET17088

16. Abstract

In the development of new and highly efficient porous electrocatalysts, two cooperative phenomena are required. The first is an increase in the electrocatalytic activity of the catalyst particle, and the second is the availability of that electrocatalyst particle for the electrochemical reaction. These two processes interact with each other in such a way that improvements in the electrochemical activity must be coupled with improvements in the availability of the electrocatalyst for reaction. Since cost effective and highly reactive electrocatalysts have been developed under this program, this report addresses the utilization of the electrocatalyst particles in the porous electrode structures. Based on the performances of the electrocatalysts in porous electrode structures, it is shown that a large percentage of the electrocatalyst in anode structures is not utilized. This low utilization translates directly and dramatically into a noble metal cost penalty for the fuel cell. Dramatic improvements in the cost effectiveness of the fuel cell will be achieved by improvements in electrocatalyst catalyzation technology and electrode structure technology.

17. Key Words (Suggested by Author(s))	18. Distribution Statement
fuel cells; electrocatalysts; electrochemical power generation; phosphoric acid	Unclassified - unlimited STAR Category 44

19. Security Classif. (of this report)	20. Security Classif. (of this page)	21. No. of Pages	22. Price*
Unclassified	Unclassified	41	

* For sale by the National Technical Information Service, Springfield, Virginia 22161

TABLE OF CONTENTS

ABSTRACT

In the development of new and highly efficient porous electrocatalysts, two cooperative phenomena are required. The first is an increase in the electrocatalytic activity of the catalyst particle, and the second is the availability of that electrocatalyst particle for the electrochemical reaction. These two processes interact with each other in such a way that improvements in the electrochemical activity must be coupled with improvements in the availability of the electrocatalyst for reaction. Since cost effective and highly reactive electrocatalysts have been developed under this program, this report addresses the utilization of the electrocatalyst particles in the porous electrode structures. Based on the performances of the electrocatalysts in porous electrode structures, it is shown that a large percentage of the electrocatalyst in anode structures is not utilized. This low utilization translates directly and dramatically into a noble metal cost penalty for the fuel cell. Dramatic improvements in the cost effectiveness of the fuel cell will be achieved by improvements in electrocatalyst catalyzation technology and electrode structure technology.

1. Objective and Scope of Work

The overall objective of this electrocatalysis program is to define the feasibility of lowering the electrocatalyst cost and to increase the activity in phosphoric acid fuel cells, as a way to increase the commercial viability of fuel cells for producing electric power.

The specific objectives of the present tasks are the preparation of a series of high surface area electrocatalysts for evaluation in phosphoric acid fuel cells. This involves fabrication of efficient gas-diffusion electrode structures and determining their electrochemical parameters for hydrogen oxidation and oxygen reduction. When possible, new experimental techniques and theoretical interpretations will be forwarded towards an understanding of the relevant electrochemical parameters.

2. Summary of Previous Work

Previously, a large number of electrocatalyst formulations were developed, starting with platinum on various carbon supports and extending to platinum with palladium for anode electrocatalysts and platinum with transition metal carbide forming elements (W, Mo, V) for cathodes. Patent disclosures on behalf of DOE have been filed and patent applications made (DOE Case S-55,310).

In order to characterize the electrocatalysts, electrochemical surface determinations were used in conjunction with x-ray crystallite size determinations and high resolution electron microscopy. Equations were then developed to correlate the platinum and the platinum alloy (or platinum intermetallic) crystallite sizes with electrochemical hydrogen adsorption data. Performances of these electrocatalysts were carried out as anodes for hydrogen oxidation and hydrogen oxidation in the presence of carbon monoxide as a function of carbon monoxide concentration and temperature. It was shown that the apparent poisoning of the electrocatalyst by carbon monoxide was significantly influenced by the electrode structure. As cathodes, performances of the electrocatalysts were obtained on air and oxygen. Further work indicated that the utilization of the electrocatalyst could be improved but the magnitude of that improvement was not known.

Since 1 MW of power generated by fuel cells can require between 3 to 5 kg of platinum, then for a conservative projection of U.S installed capacity of 15,000 MW cumulative through the year 2000 and an equal amount worldwide, there is a requirement between 90,000 and 150,000 kg of platinum. This translates to a platinum dollar requirement between $1,296,000,000 and $2,160,000,000 (1981 base). The present program has contributed in a potential catalyst cost savings of between $259,200,000 and $432,000,000 (1981 base). Considering the indications of low utilization of catalyst in electrode structures, then the potential savings in catalyst cost to the year 2000 would be significantly greater than the catalyst cost savings so far demonstrated.

3. Technical Progress

3.5. Task 5 - Preparation of Platinum-Based Carbon-Supported Electrocatalysts

During this quarter a number of electrocatalysts were prepared, investigating the preparation of platinum-vanadium intermetallics on Consel. In addition, the formation of platinum-tungsten compounds was carried out by forming tungsten carbide on the surface of Consel I, and then catalyzing with platinum. The tungsten carbide was formed by impregnating the Consel I with ammonium tungstate, heating to 700°C and passing a small amount of carbon monoxide (see D. E. Fornwalt, E. J. Felton and P. Stonehart, Micron 1975, 6, 147-152). After the carbon monoxide treatment, the tungsten carbide on the carbon support was heat treated for a further 16 hours at 700°C in argon. After heat treatment, the tungsten carbide on carbon was catalyzed with platinum using a colloidal technique.

The electrocatalyst designations, electrode numbers and composition are given in Table I.

TABLE I

Catalyst #	Electrode #	Composition	
EC-158	P-113	10% PT/WCI	2.5% WC/Consel I
EC-159	P-114	10% Pt/WCI	5.0% WC/Consel I
EC-160	P-115	10% Pt/WCI	10.0% WC/Consel I

In addition, a small number of electrocatalysts were prepared in order to investigate the influence of PGM loading on the electrode performance. At this time there are two types of carbon supports that have been investigated. These are Vulcan XC-72R, a turbostratic furnace black that is easy to catalyze and to form into electrode structures, and the Consel I, which is a steam-treated acetylene black having a partially "graphitized" surface layer. The latter carbon is more difficult to catalyze and to form into electrode structures due to the graphitic nature of the carbon surface. In order to maintain approximately the same PGM particle sizes, the carbons were catalyzed using our standard colloidal technique. All of the catalyst formulations were treated in the same manner. The electrocatalyst designations, electrode numbers and compositions are given in Table II.

TABLE II

Catalyst #	Electrode #	
EC-123	P-116	50/50 a/o Pt-Pd on Consel I 4 w/o PGM 0.2 mg PGM/cm^2 electrode
EC-161	P-117	1 w/o Pt on Vulcan XC-72R 0.05 mg Pt/cm^2 electrode
EC-162	P-118	4 w/o Pt on Vulcan XC-72R 0.2 mg Pt/cm^2 electrode
POWERCAT 1000	P-91	10 w/o Pt on Vulcan XC-72R 0.5 mg Pt/cm^2 electrode

3.7. Task 7 - Catalytic Activity of Platinum-Based Carbon-Supported Electrolytes

A number of catalyst preparations were formed into gas diffusion electrode structures and run in 100% phosphoric acid at 180°C as oxygen and air electrodes. In particular, the electrocatalyst performance for the platinum-vanadium intermetallic supported on Consel IV were determined. The characteristics of these electrocatalyst compositions were reported in the last quarterly report (July-September 1981). TableIII shows the catalyst designations, electrode numbers, and the apparent platinum surface area pre-test and post-test.

TABLE III

Catalyst #	Electrode #	Composition	Pre-Test	Post-Test
EC-154	P-108	0.54 mg Pt-V/cm^2 electrode 10.8% Pt-V/Consel IV	80 m^2/g	88 m^2/g
EC-155	P-109	0.27 mg Pt-V/cm^2 electrode 10.8% Pt-V/Consel IV	90 m^2/g	77 m^2/g
EC-157	P-112	0.27 mg Pt-V/cm^2 electrode 5.4% Pt-V/Consel IV	105 m^2/g	88 m^2/g

Comparative performance data are shown in Figure 1 for electrodes P-109 and P-112 on oxygen and air. Although reasonable linearity is obtained for the Tafel plots, we are still concerned about the significance of this linearity, since it is not truly diagnostic of the electron transfer reaction. The Tafel slope on oxygen is of the order of 105-110 mV, which we think is high and gains are indicated that are yet to be made with improvements in the electrode structure. Nevertheless, these electrodes and electrocatalysts show promise since the

Consel IV support is a high surface area graphitized carbon that has been doped substitutionally with another element. Patents are in the process of being filed for this support by EPRI since it was conceived and developed under their funding. Patent disclosures on the catalyzation and application of the electrocatalyst are being submitted to DOE under this program.

Figure 2 shows comparative performance data for electrodes P-108 and P-109. It can be seen that P-108 shows excellent performance when compared to previous platinum-vanadium intermetallics on carbon supports. It should be pointed out that the performance curves for P-108 and P-109 are obtained on electrodes containing different loadings of platinum. Electrocatalyst EC-154 in electrode 108 has twice the loading of EC-155 in electrode P-109. This higher loading is reflected in the higher current densities that are seen.

Figure 3 is a composite plot of the platinum-tungsten electrocatalysts supported on Consel I. The designations are given in the legend of the figure. In general, the results have been disappointing initially but very little effort has been put forward in optimizing and controlling the formation of tungsten carbide. It is known that the process for reduction of the tungsten oxide to tungsten carbide does produce some excess carbon and it is not known whether alloy formation between tungsten and platinum has occurred. At first glance, it would seem that there is significant surface segregation by the tungsten with concomitant burying of the platinum, and hence, loss of electrocatalyst activity. Some indication that this may be so is shown by the pre- and post-test platinum surface areas that were obtained on electrode P-113. In this instance, the pre-test surface area on platinum was 160 m^2/g and the post-test surface area was 65 m^2/g. Such a large decrease likely indicates that the platinum atoms are being buried in the electrocatalyst rather than migration and growth of platinum crystallites. Clearly, further work should be done to understand in more detail surface segregation between the platinum group metals (PGMs) and refractory elements as electrocatalysts. In order to unravel the influence of electrode structure, electrocatalyst activity, kinetic effects due to PGM compositions, and the influence of the carbon supports, it was decided that detailed adsorption isotherms would be developed using the poisoning reaction of carbon monoxide on the hydrogen oxidation reaction. This approach extends some of the pioneering work that was done previously using carbon monoxide as a probe for the hydrogen oxidation reaction on flooded platinum black electrode structures (see P. Stonehart and P. N. Ross, Catalysis Reviews, 1975, 12, 1-35, and P. Stonehart and P. N. Ross, Electrochim. Acta, 1976, 21, 441-445).

To provide an understanding for the operation of gas diffusion electrodes, it was reasonable that the influence of temperature over the range 120-210°C be evaluated together with the influence of the carbon monoxide poison as a probe over the range 0% CO to 5% CO. Earlier, such an examination had been carried out on the platinum-palladium low loaded alloy designated EC-123 (P-116). Those performance curves and the catalyst diagnostics had been shown in our 7th Quarterly Report (CR165519). The work in this report is a continuation and extension of that work.

It should be recognized that although we had indicated that the key carbon monoxide poisoning concentration in the anode gas stream for steam reformed methanol was 0.5% carbon monoxide, it is fortuitous that the latest fuel mixture for steam reforming and shifting of hydrocarbons in United Technologies' pressurized power plant at 120 psia is 70% hydrogen, 1% carbon monoxide and 29% carbon dioxide (Quarterly Report #4, Contract DEN-3-191, February 1, 1981-April 30, 1981). Clearly, the results that we are presenting are exactly targeted on <u>both</u> steam reformed methanol and steam reformed and shifted hydrocarbons for the UTC pressurized fuel cell.

All data were obtained in our test stands, allowing 16 hours after electrode insertion for the electrocatalyst layer to fill. The high performance BC 1200 potentiostats with automatic IR correction and compensation were used. All of the electrodes were of the same thickness and contained the same amount of Teflon. All electrodes were sintered at the same temperature. Performance data for this series are shown in Figures 4 through 15 for the electrodes P-117, P-118 and P-91. Performance data for electrodes P-116 were given previously (7th Quarterly Report, CR165519, Figures 5 through 8).

In order to derive the apparent isotherms for carbon monoxide poisoning of the hydrogen reaction on the platinum or PGM electrocatalyst surface, comparisons were made between the rate of the hydrogen oxidation reaction on an unpoisoned surface and that performance attained for the same hydrogen partial pressure in the presence of different partial pressures of carbon monoxide at the same potential (20 mV). A tabulation is given in Table IV for these <u>apparent</u> isotherms together with tabulations from the electrodes P-116. The apparent available surface areas ($1-\theta_{CO}$) as a function of carbon monoxide concentration and temperature are shown in Figure 16. Apparent Arrhenius relationships will not be shown at this time since the first derivations were done previously (see 7th Quarterly Report, CR165519, Figure 11).

Not all of the hydrogen entering the fuel cell anode can be oxidized, since the degree of consumption is related to the operating potential. At 180°C with 20 mV polarization (vs RHE) the surface equilibrium partial pressure due to the Nernst relationship is 0.35 at. Since the incoming partial pressure for hydrogen is 0.75 at. (giving an open circuit potential of 5.5 mV at 180°C), then the available hydrogen concentration differential is 0.4 at. which must support the electrocatalytic reaction rate.

In order to ascertain whether or not the adsorption isotherms in Figure 16 are truly representative of the adsorption equilibrium kinetics in the absence of diffusion, one has to perform other analyses of the data. It is well known that at low reaction rates, kinetic parameters are dominant, whereas at high reaction rates, diffusion interferences are obtained so that the reaction rate is no longer directly proportional to the catalyst surface area or even the catalyst loading. This enters into the dimension of catalyst utilization and effectiveness factor. It is not our purpose in this monthly report to enter into detailed discussions of effectiveness factors for electrocatalysts at this time. Suffice to say, for a given catalyst particle size, the reaction rate should double if the catalyst particle density also doubles. If the catalyst particle density increases manyfold (or the catalyst active area increases manyfold), we should observe a concomitant increase in the reaction rate. If the reaction <u>does not increase</u> by the surface area increase multiple, then diffusion limitations are indicated and the catalyst utilization is low. One approach is to determine specific reaction rates on low loaded electrodes and compare those reaction rates with electrodes at higher loadings. Since we have taken care to catalyze the electrode materials with uniform metal particles by means of a colloidal deposition process, then the variation in electrocatalyst surface area is reflected in the variation in the number of particles which is controlled by the metal loading. Two sets of data are plotted in Figures 17 and 18. In Figure 17 the current density is shown for hydrogen oxidation at 210°C in the absence of a poison as a function of the catalyst loading. It is clear that the low loaded electrocatalyst (which is 1 w/o Pt on carbon) is nearly as active as the 10 w/o Pt on carbon. Since the current density would be 0 at 0 w/o PGM on carbon, we are allowed to extrapolate through the lowest loading datum to anticipate the current density that would be obtained at higher loadings with efficient utilization of the catalyst. It is clear that even at 4 w/o PGM, the current density that should be observed is at least two or three times greater than is obtained.

This means that at least 70% of the catalyst is not being utilized. From examination of the performance curves, for hydrogen oxidation in the presence of carbon monoxide at the 1% level and at 180°C, we may construct Figure 18. The multiple of the increase in current density between the 1 w/o Pt and 10 w/o Pt does not reflect the increase in surface area on the electrocatalyst or the increase in the loading by the platinum. If we assume (reasonably) that at constant temperature the true CO poisoning isotherm on the metal particle surface does not change, then the current density on the 10 w/o Pt electrocatalyst should be ten times that of the 1 w/o Pt on carbon electrocatalyst (if the catalyst particles have the same size). It may be that there are diffusion effects even at the 1 w/o Pt level but further data must be obtained to support that contention.

Extrapolating from the current density that is obtained on the 1 w/o electrocatalyst to the 4 w/o PGM on carbon electrocatalyst shows that the current densities expected would be at least two to three times greater than have been observed. Significant gains in catalyst utilization are yet to be made.

We can make a rough estimate for the maximum current density that should be derived with 0.4 at. hydrogen partial pressure differential (40% H_2 utilization) at 180°C in 100% H_3PO_4. At 20 mV polarization, the hydrogen evolution reaction (reverse reaction) decreases and the free surface for dissociation of the hydrogen molecule (Tafel reaction) increases. A dispersed platinum electrocatalyst of 60 m^2/g Pt (which is not as high as our electrocatalysts studied here) will have a surface of 600 cm^2/mg Pt. Since the exchange current for hydrogen molecule oxidation on platinum in acid is 20 mA/cm^2 (P. Stonehart, J. Electroanal. Chem., 1977, 77, 245-248), then at room temperature in dilute acid, the kinetic limitation (exchange current) becomes at least 12,000 mA/mg Pt.

With increase in temperature, the hydrogen dissociation reaction rate increases by 4 kcal/mole but the gas solubility can be expected to decrease by an equal magnitude.

These estimates show that current densities of 1,200 mA could be expected for hydrogen molecule oxidation on 0.1 mg Pt having only 60 m^2/g surface area, provided that all of the platinum electrocatalyst was utilized. With a hydrogen utilization of 40% (see before) the estimates of kinetically limiting current densities are then 480 mA/0.1 mg Pt. Figure 17 shows a hydrogen oxidation current of 350 mA/0.1 mg Pt at 210°C and 20 mV. This electrocatalyst has a surface area higher than 60 m^2/g but the exact solubility of hydrogen is an unknown. Even though the

inexact calculation given here is close to the observed measurement, the platinum utilization is probably still low and the real kinetic limitation for hydrogen molecule oxidation may be twice the value so far observed.

Although the results presented so far have been obtained on hydrogen oxidation, using CO poisoning as the probe, it is important to note that these conclusions are truly applicable to oxygen molecule reduction at the cathode also. Since the same electrode structures (and in some cases actual electrodes) have been used historically to obtain both andoe and cathode data, it is important to note that at the current density and electrocatalyst loading where diffusional effects are noted for the anode, then at the same current densities approximately the same diffusional interferences will be obtained. It is true that at the anode the hydrogen molecule oxidation reaction is a two electron process, whereas at the cathode the oxygen molecule reduction reaction is a four electron process. The flux of the reacting molecules through the liquid electrolyte film is related to the product of the molecule solubility and diffusivity and since both molecules in the electrolyte are non-polar, the solubility trends of the gas molecules in aqueous electrolytes at the same temperature are expected to be similar. On the other hand, the diffusivity of hydrogen in aqueous solutions is twice that of the oxygen molecule (see "Physicochemical Hydrodynamics" V. G. Levich, Prentice-Hall, N.J., 1962, p. 325, and K. Klinedinst, J. A. S. Bett, J. MacDonald, and P. Stonehart, Journal of Electroanalytical Chemistry, 57 (1974) 281-289). The sum total of this discussion shows that although the overall electron transfer for the hydrogen molecule oxidation reaction is one-half that of the oxygen molecule reduction reaction, the diffusivity is twice as great so that at the same current densities in gas diffusion electrodes where diffusion played a role, the mass transfer characteristics that are seen at the anode will be reflected in an identical way at the cathode. It can be concluded, therefore, that if the catalyst utilization at the anoce is less than 30% for a 4 w/o electrocatalyst and is less than 10% for a 10 w/o catalyst, then the same utilizations will be obtained at the cathodes for the same catalyst loadings.

In order to evaluate the operation of gas-diffusion electrode structures, some fundamental information is required regarding the solubility and diffusivity of the reacting gas molecules in the electrolyte environment. When coupled with estimates of the thicknesses of the electrolyte films on the electrocatalysts and an understanding of the electrocatalyst structure, then operation of the electrode may be understood more fully and subjected to further development.

Information on solubility and diffusivity of oxygen in hot concentrated phosphoric acid is given in the Klinedinst paper up to 150°C and 96% H_3PO_4. From Figure 2 of that paper, the solubility-diffusivity product for oxygen in 100% phosphoric acid, together with temperature dependence of the D_OC_O product can be extrapolated. That relationship is shown in Figure19 , which is particularly interesting since the D_OC_O product increases linearly with temperature. There is no other information on the related solubility-diffusivity of hydrogen.

In order to explore the effect of electrode preparation technology on electrocatalyst utilization, a series of electrodes were prepared where the sintering time for the Teflon was extended. Since it had been shown previously that the thermal sintering of Teflon in contact with carbon blacks produced degradation and flow of the Teflon polymer (K. A. Klinedinst, W. M. Vogel and P. Stonehart, J. Materials Science, 1976 11, 794-800), it was reasoned that the electrode film thickness could be lowered by thinning the Teflon coating on the carbon. Table IV Electrode P-119, contains 4 w/o platinum on Consel I (EC-124) with 30% PTFE sintered 10 minutes at 315°C. Electrode P-119S is the same as P-119 except that the sintering time at 315°C was 40 minutes. Electrode P-121 contained 10 w/o platinum on Consel I with 30% PTFE sintered for 10 minutes at 315°C. The influence of temperature and carbon monoxide partial pressure on the apparent electrocatalyst surface available for hydrogen molecule oxidation is included in Table IV. Analyses of the performance results are included in Figure 17 for hydrogen oxidation at 210°C in the absence of carbon monoxide and in Figure 18 for hydrogen oxidation at 180°C in the presence of 1% carbon monoxide. Preliminary conclusions show that the utilization of the electrocatalyst is low in all instances, but that with extended sintering of the Teflon the utilization increases. We do not have sufficient data with many electrodes to know the degree of performance scatter. Further work in this direction will clearly be fruitful.

4. Changes

There are no changes in the program.

5. Problem Areas

There are no problem areas at this time.

TABLE IV

Influence of Temperature and Carbon Monoxide Partial Pressure on Apparent Electrocatalyst Surface Available for Hydrogen Molecule Oxidation

P-116

Gas Mix of 75% H_2 Plus (Balance N_2)	Current Density (mA) at 20 mV Polarization							
	120°C		150°C		180°C		210°C	
		$1-\theta_{CO}$		$1-\theta_{CO}$		$1-\theta_{CO}$		$1-\theta_{CO}$
0% CO	181	1.0	270	1.0	420	1.0	470	1.0
0.5% CO	58	.32	140	.52	230	.55	390	.83
1% CO	33	.18	115	.43	205	.49	375	.80
2% CO	24	.13	100	.37	165	.39	330	.70
5% CO	21	.11	72	.27	135	.32	280	.60

P-117

0% CO	200	1.0	260	1.0	300	1.0	360	1.0
0.5% CO	11	.055	100	.38	145	.48	320	.88
1% CO	7	.035	52	.20	130	.43	290	.80
2% CO	5	.025	35	.135	110	.36	260	.72
5% CO	3.4	.017	22	.085	92	.31	200	.55

P-118

0% CO	235	1.0	300	1.0	315	1.0	350	1.0
0.5% CO	45	.19	160	.53	240	.76	305	.87
1% CO	30	.13	140	.47	225	.71	300	.85
2% CO	20	.085	110	.37	200	.63	295	.48
5% CO	13	.055	76	.25	170	.54	270	.77

P-91

0% CO	240	1.0	320	1.0	420	1.0	500	1.0
0.5% CO	56	.23	200	.63	320	.76	400	.8
1% CO	32	.13	170	.53	300	.71	385	.77
2% CO	26	.11	150	.47	280	.67	365	.73
5% CO	20	.08	120	.38	250	.59	350	.70

TABLE IV (Continued)

Influence of Temperature and Carbon Monoxide Partial Pressure on Apparent Electrocatalyst Surface Available for Hydrogen Molecule Oxidation

P-119

Gas Mix of 75% H_2 Plus (Balance N_2)	Current Density (mA) at 20 mV Polarization							
	120°C		150°C		180°C		210°C	
		$1-\theta_{CO}$		$1-\theta_{CO}$		$1-\theta_{CO}$		$1-\theta_{CO}$
0% CO	220	1.0	320	1.0	340	1.0	370	1.0
0.5% CO	38	.17	140	.44	270	.79	330	.89
1% CO	27	.12	120	.37	250	.73	320	.86
2% CO	20	.09	110	.34	220	.65	280	.76
5% CO	14	.06	80	.25	200	.59	260	.70

P-119S

0% CO	230	1.0	280	1.0	380	1.0	430	1.0
0.5% CO	39	.17	150	.53	290	.76	370	.86
1% CO	29	.12	135	.48	270	.71	350	.81
2% CO	22	.09	120	.43	240	.63	320	.74
5% CO	16	.07	80	.29	220	.58	280	.65

P-121

0% CO	230	1.0	320	1.0	380	1.0	400	1.0
0.5% CO	58	.25	200	.62	320	.84	380	.95
1% CO	38	.17	160	.50	280	.74	360	.90
2% CO	30	.13	115	.36	260	.68	340	.85
5% CO	10	.04	100	.31	240	.63	320	.80

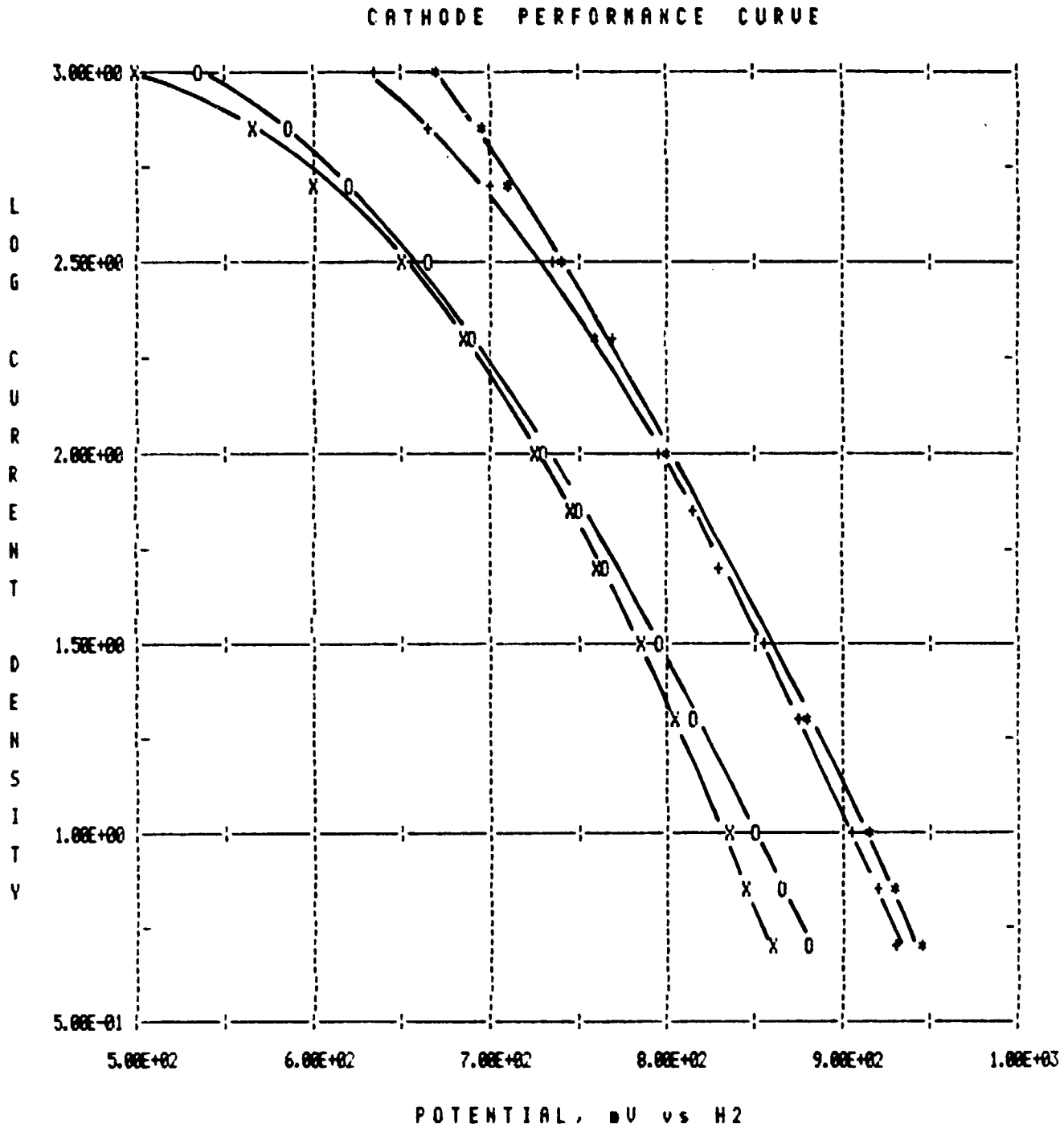

Figure 1.

Oyxgen and air performance curves in 100% phosphoric acid 180^{o}C, iR corrected. Electrode P-109 oxygen (*), air (0). Electrode P-112 oxygen (+), air (X). Nominal Pt-V loading is 0.27 mg/cm^{2} electrode.

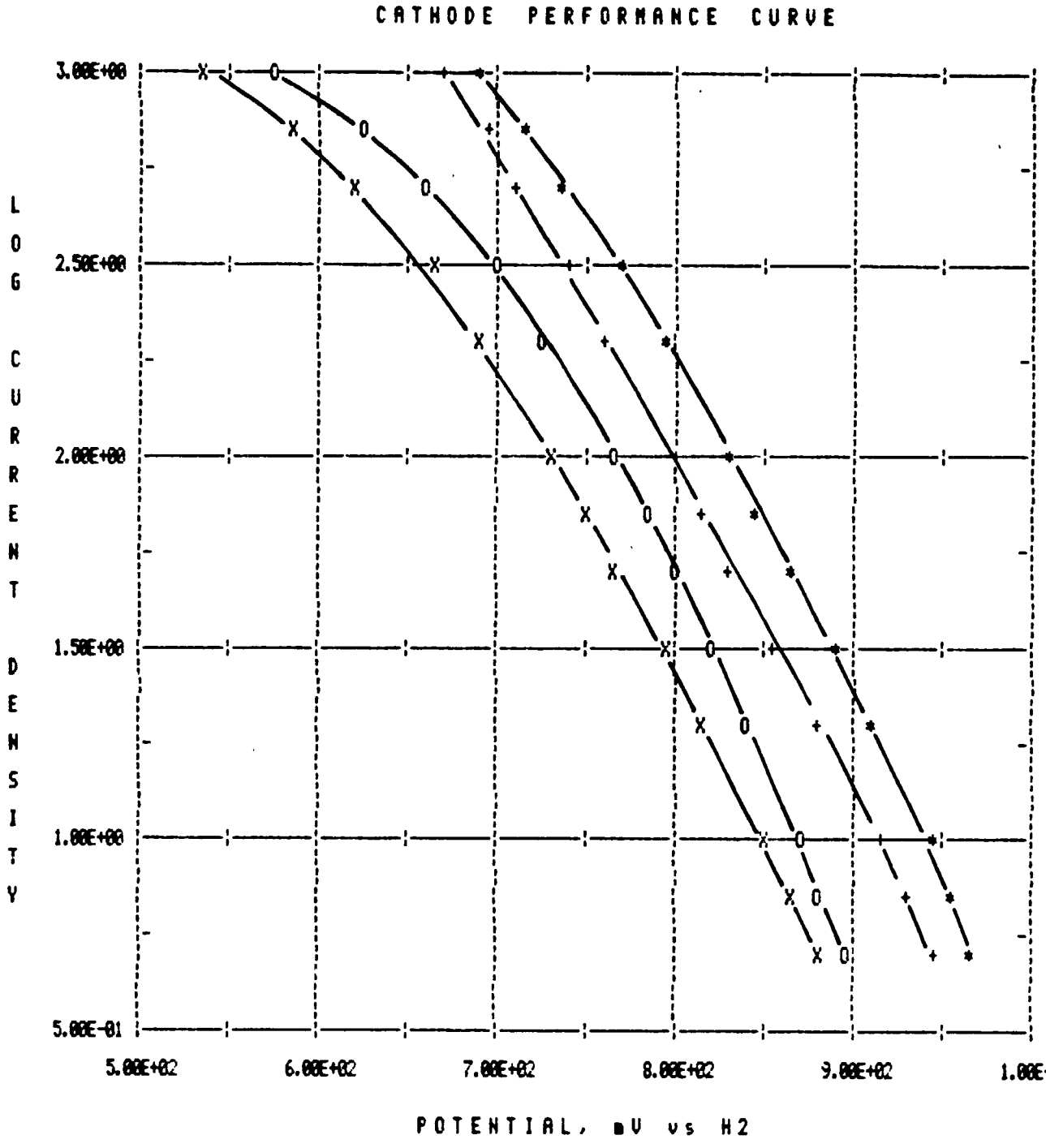

Figure 2.

Oxygen and air performance curves in 100% phosphoric acid 180°C, iR corrected. Electrode P-108 oxygen (*), air (0). Electrode P-109 oxygen (+), air (X). P-108 .54 mg Pt-V/cm^2 electrode. P-109 0.27 mg Pt-V/cm^2 electrode.

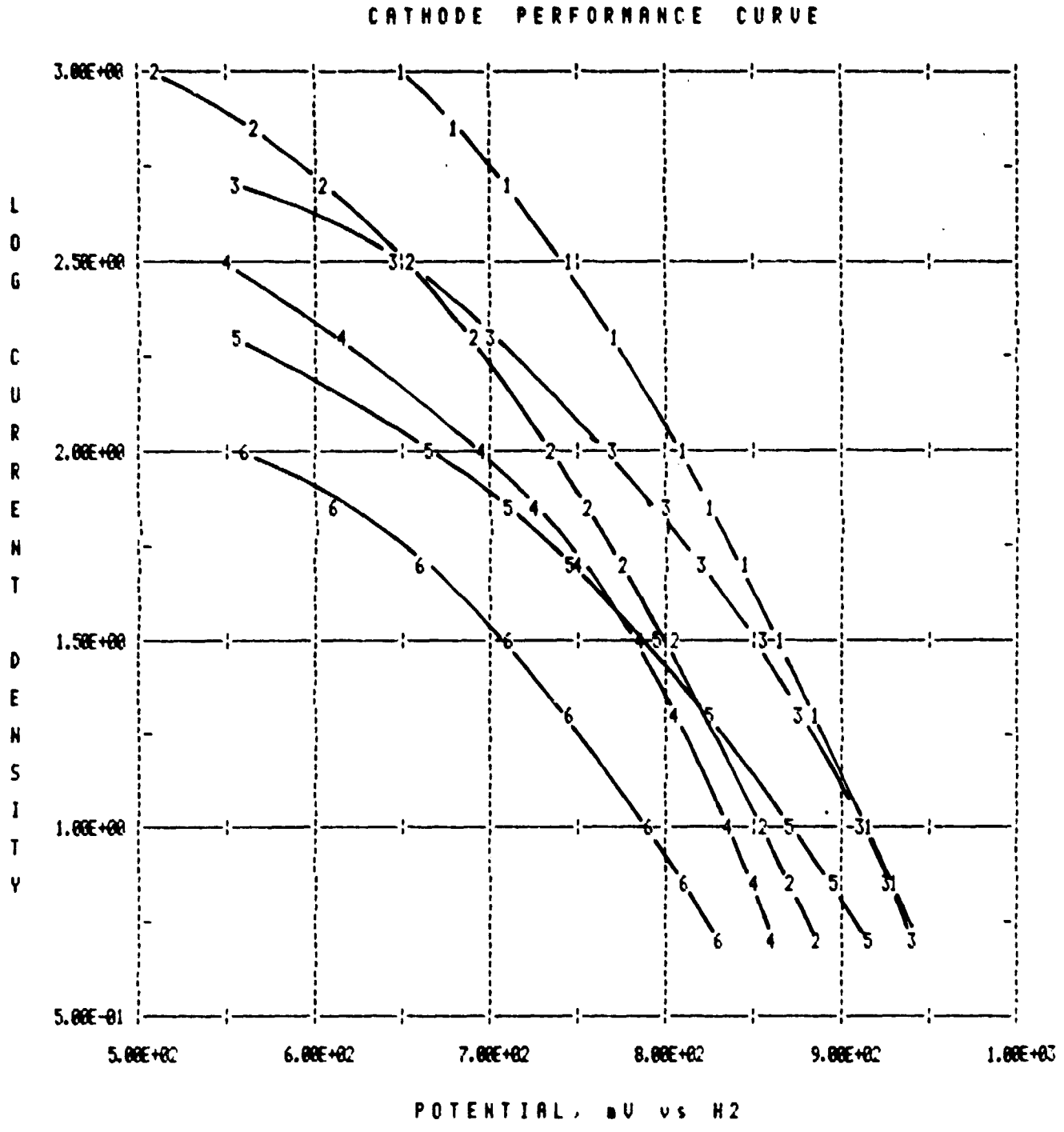

Figure 3.

Oxygen and air performance curves in 100% phosphoric acid 180°C, iR corrected. Electrode P-113 oxygen (1), air (2). Electrode P-114 oxygen (3), air (4). Electrode P-115 oxygen (5), air (6). All electrodes contain 0.5 mg Pt/cm^2.

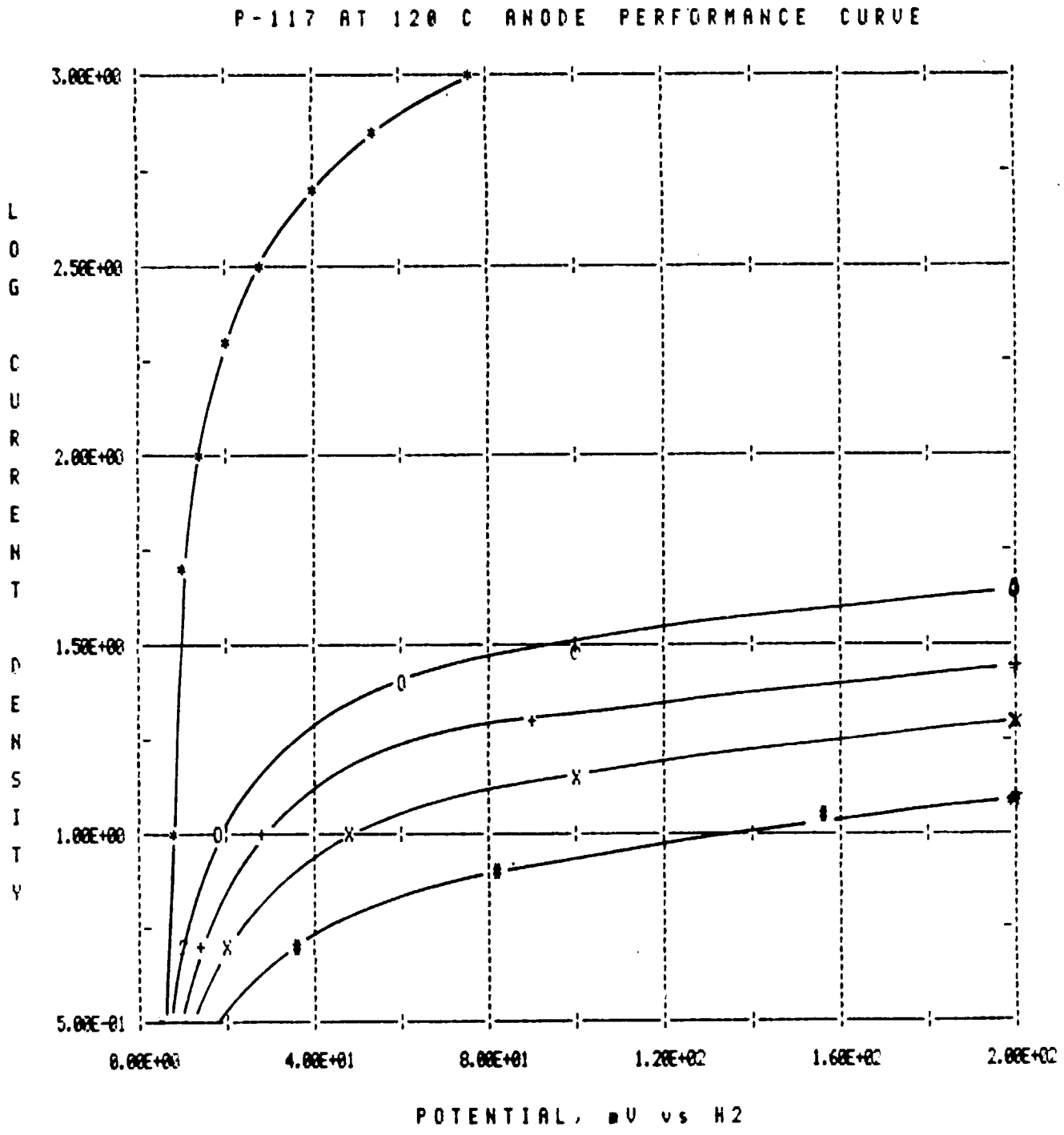

FIGURE 4.

Electrode P-117 at 120°C. 1 w/o Pt on Vulcan XC-72R, 0.05 mg Pt/cm^2 electrode. 100% H_3PO_4. All data corrected for iR. Gas mixtures 75% H_2, balance N_2 with 0% CO (*); 0.5% CO (0); 1% CO (+); 2% CO (X) and 5% CO (#).

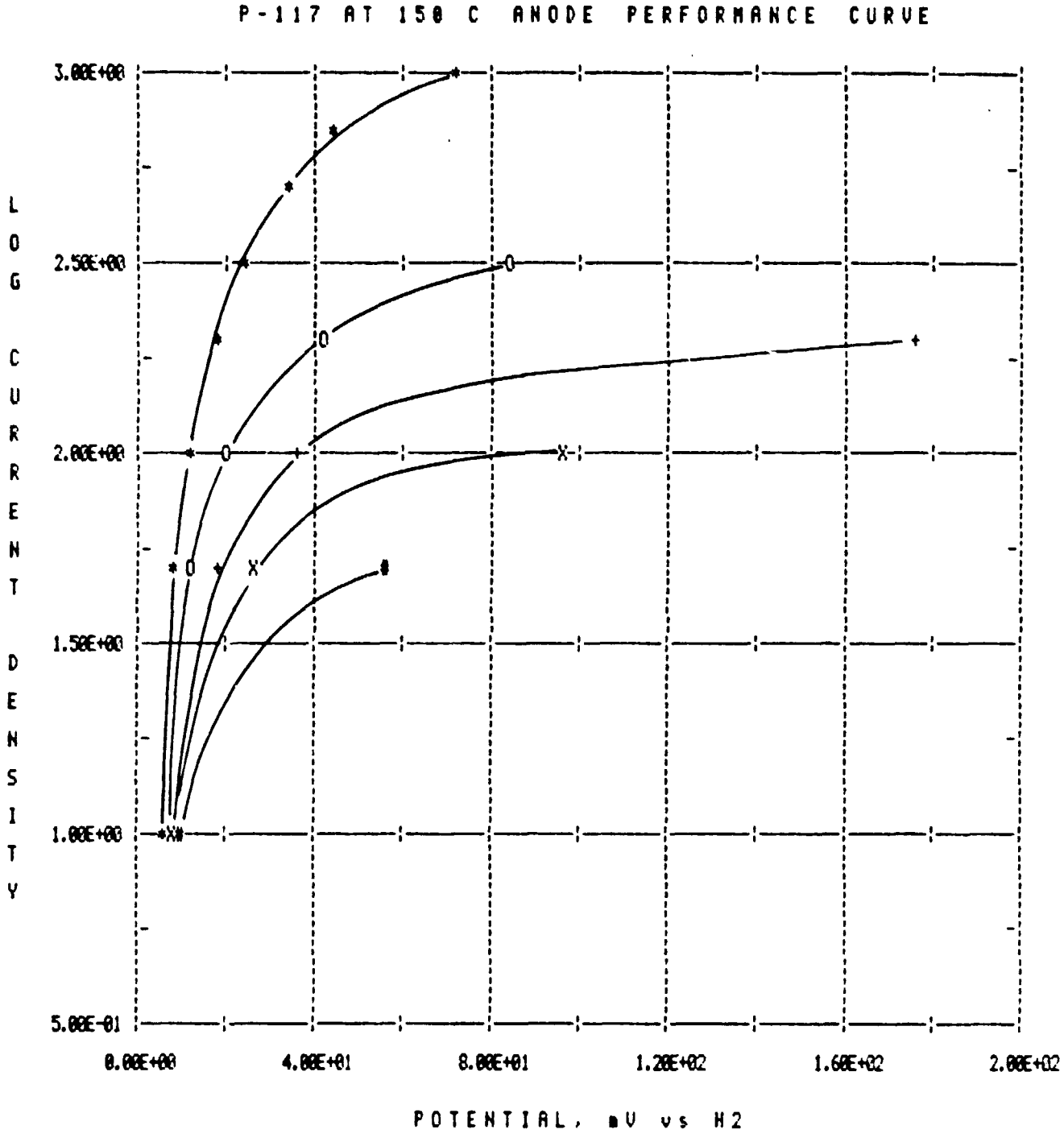

FIGURE 5.

Electrode P-117 at 150°C. 1 w/o Pt on Vulcan XC-72R, 0.05 mg Pt/cm^2 electrode. 100% H_3PO_4. All data corrected for iR. Gas mixtures 75% H_2, balance N_2 with 0% CO (*); 0.5% CO (0); 1% CO (+); 2% CO (X) and 5% CO (#).

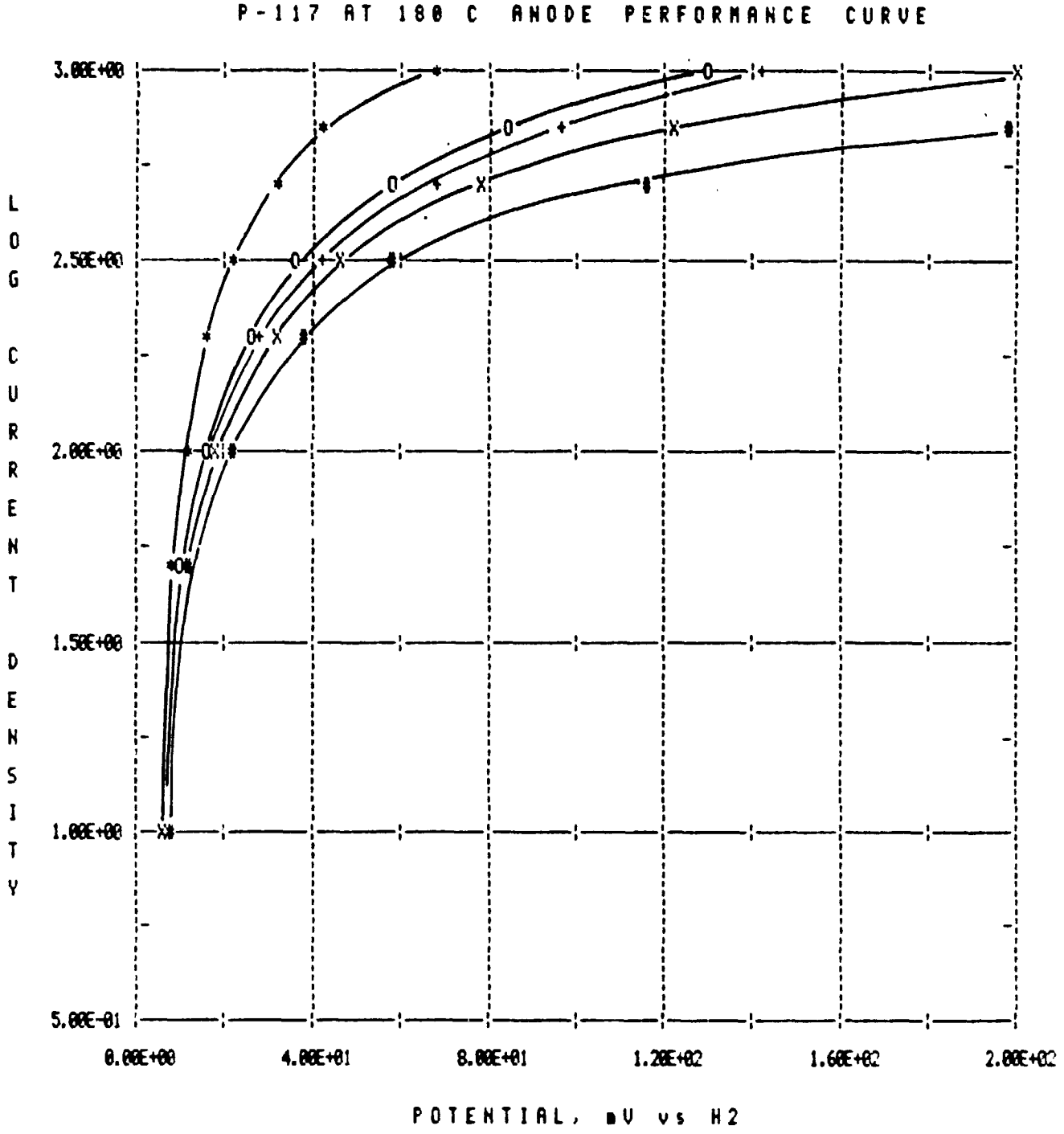

FIGURE 6.

Electrode P-117 at 180°C. 1 w/o Pt on Vulcan XC-72R, 0.05 mg Pt/cm^2 electrode. 100% H_3PO_4. All data corrected for iR. Gas mixtures 75% H_2, balance N_2 with 0% CO (*); 0.5% CO (0); 1% CO (+); 2% CO (X) and 5% CO (#).

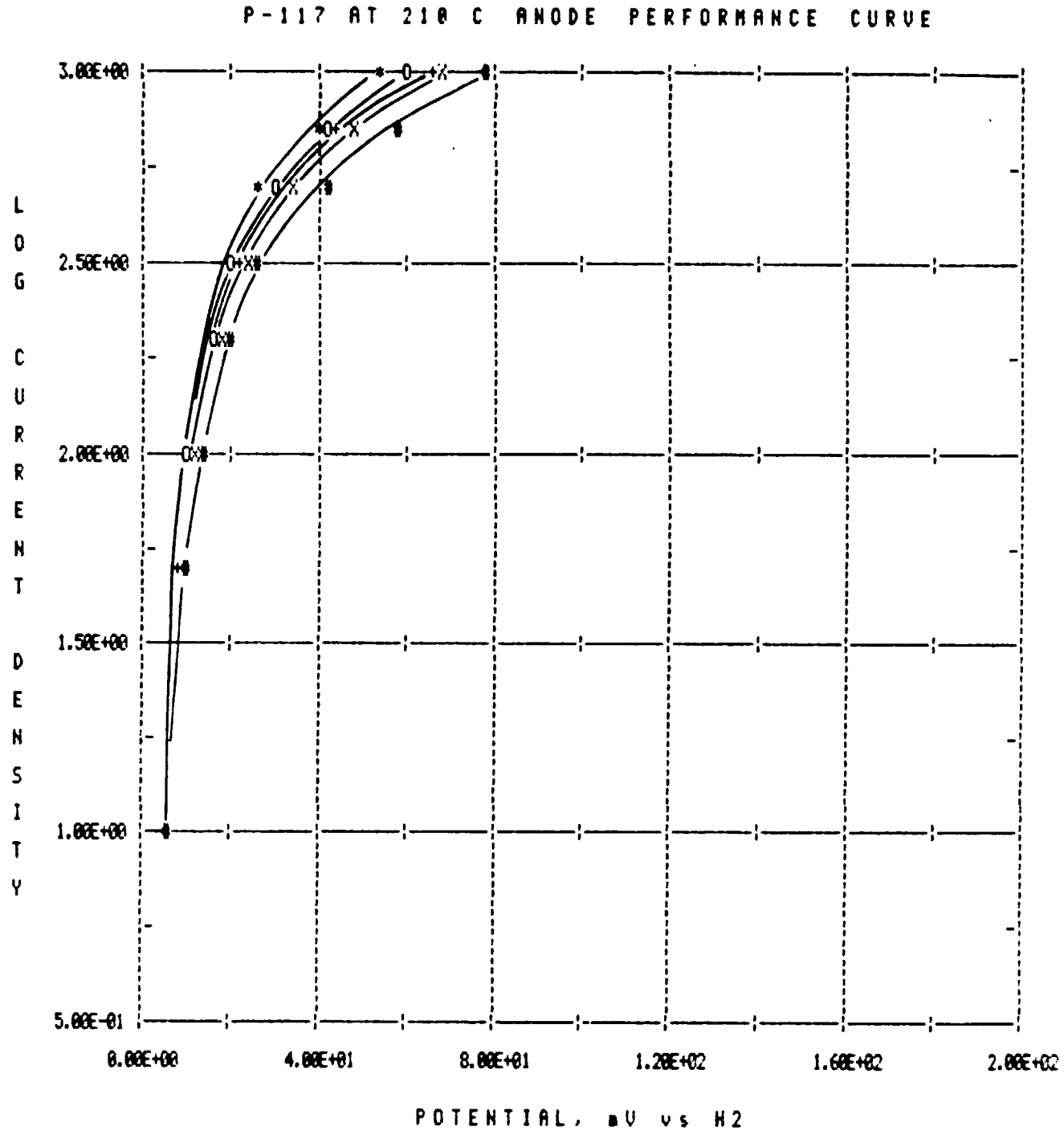

FIGURE 7.

Electrode P-117 at 210°C. 1 w/o Pt on Vulcan XC-72R, 0.05 mg Pt/cm^2 electrode. 100% H_3PO_4. All data corrected for iR. Gas mixtures 75% H_2, balance N_2 with 0% CO (*); 0.5% CO (0); 1% CO (+); 2% CO (X) and 5% CO (#).

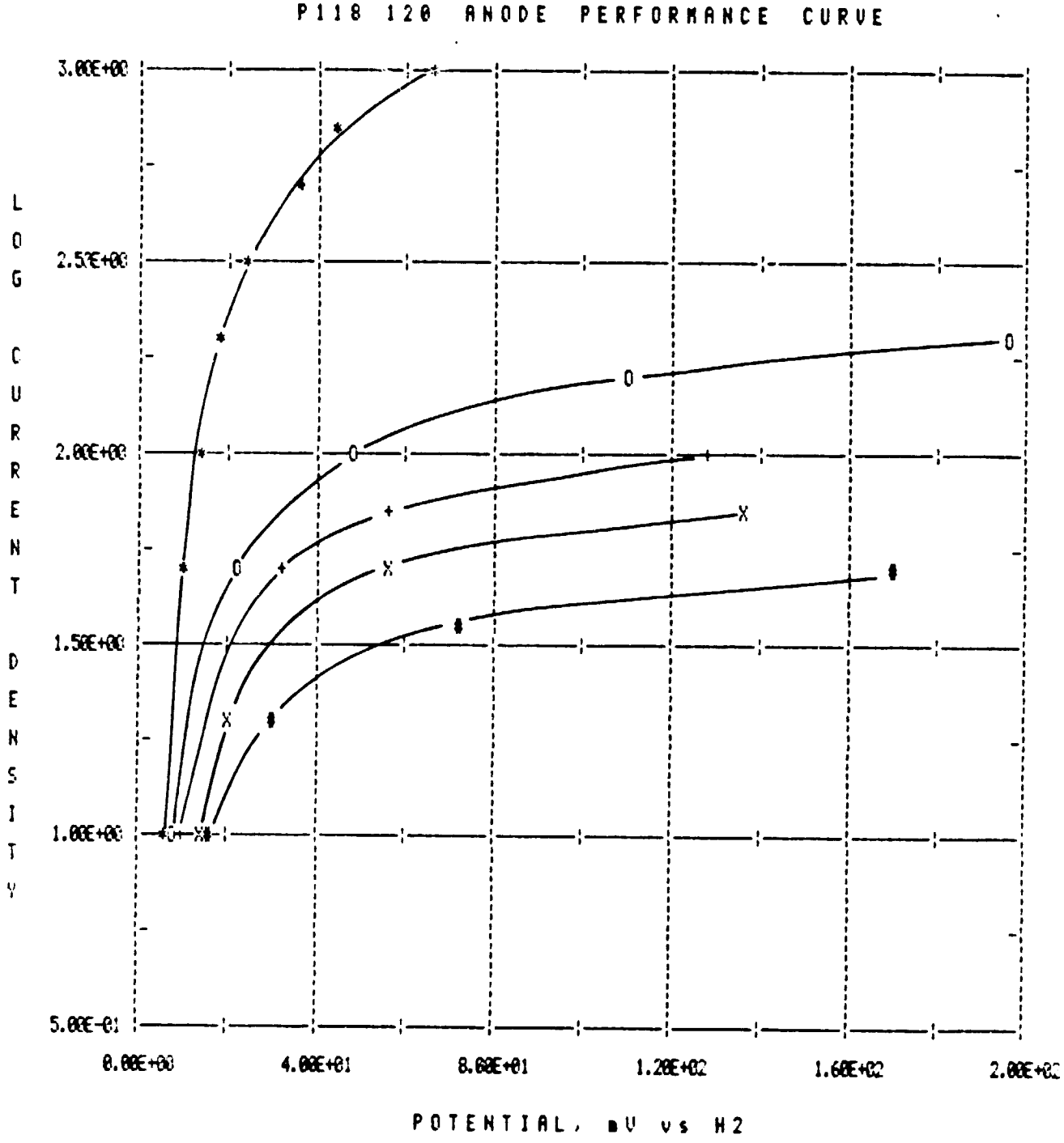

FIGURE 8.

Electrode P-118 at 120°C. 4 w/o Pt on Vulcan XC-72R, 0.2 mg Pt/cm^2 electrode. 100% H_3PO_4. All data corrected for iR. Gas mixtures 75% H_2, balance N_2 with 0% CO (*); 0.5% CO (0); 1% CO (+); 2% CO (X) and 5% CO (#).

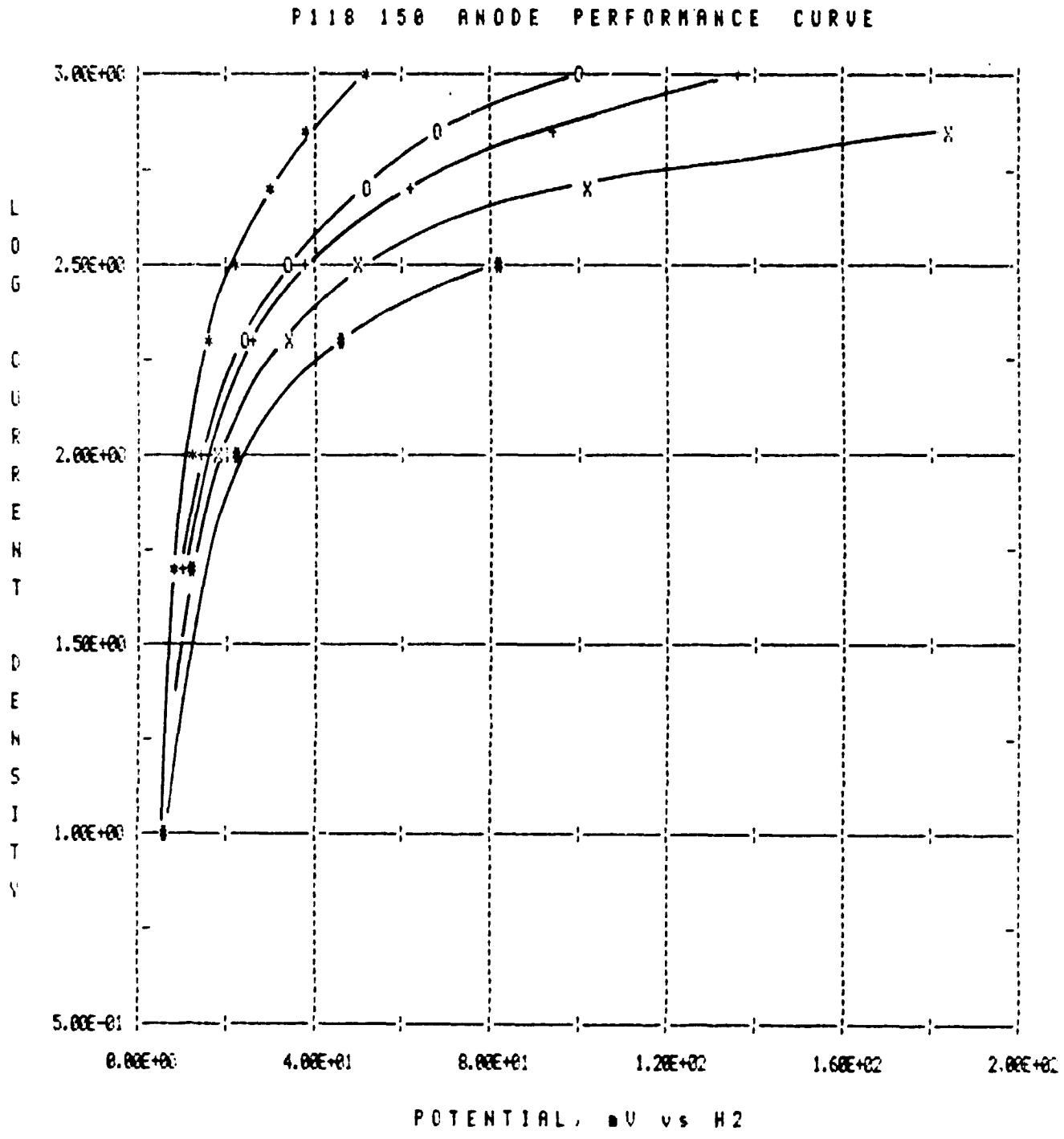

FIGURE 9.

Electrode P-118 at 150°C. 4 w/o Pt on Vulcan XC-72R, 0.2 mg Pt/cm^2 electrode. 100% H_3PO_4. All data corrected for iR. Gas mixtures 75% H_2, balance N_2 with 0% CO (*); 0.5% CO (O); 1% CO (+); 2% CO (X) and 5% CO (#).

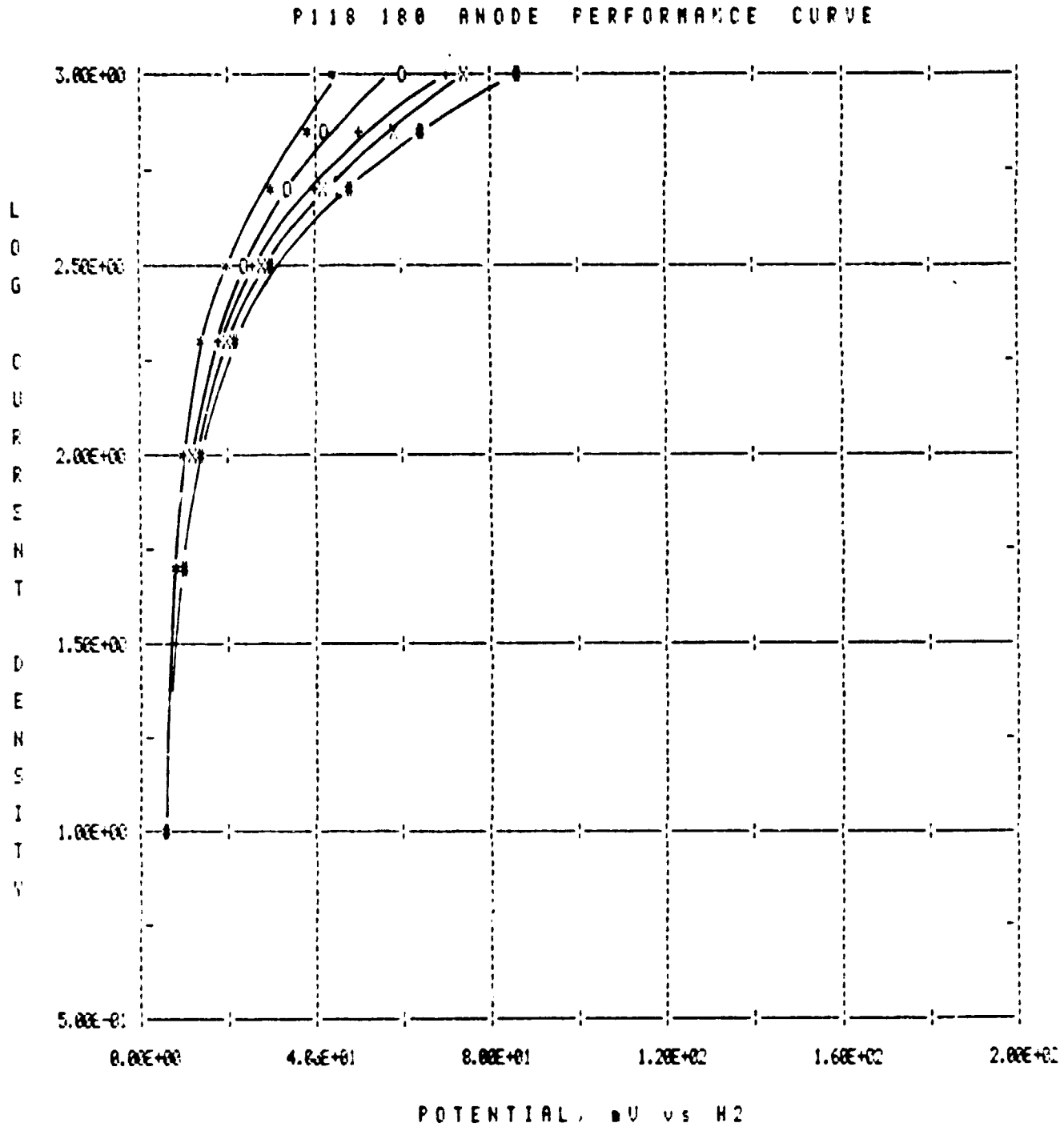

FIGURE 10.

Electrode P-118 at 180°C. 4 w/o Pt on Vulcan XC-72R, 0.2 mg Pt/cm^2 electrode. 100% H_3PO_4. All data corrected for iR. Gas mixtures 75% H_2, balance N_2 with 0% CO (*); 0.5% CO (0); 1% CO (+); 2% CO (X) and 5% CO (#).

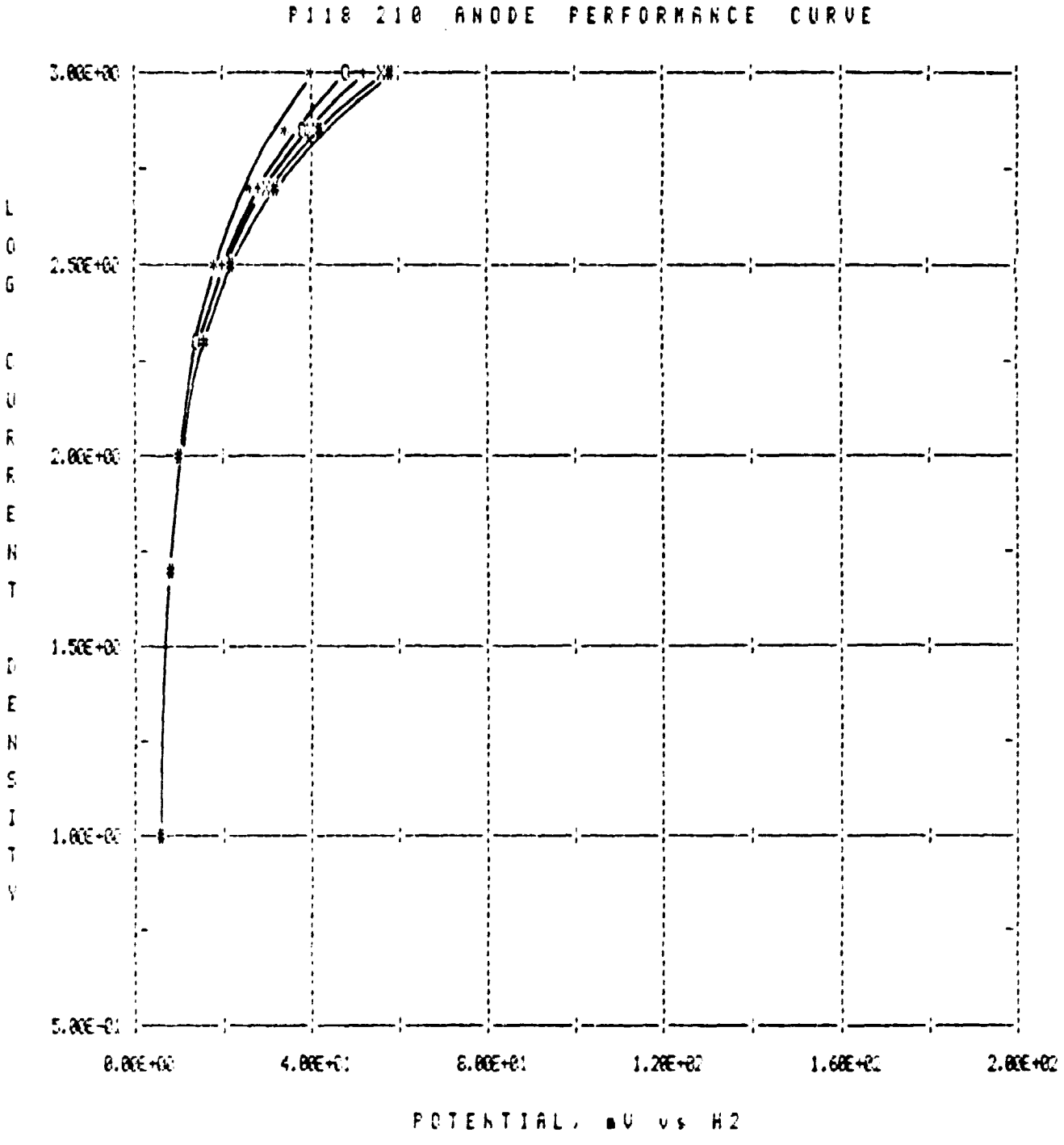

FIGURE 11.

Electrode P-118 at 210°C. 4 w/o Pt on Vulcan XC-72R, 0.2 mg Pt/cm^2 electrode. 100% H_3PO_4. All data corrected for iR. Gas mixtures 75% H_2, balance N_2 with 0% CO (*); 0.5% CO (0); 1% CO (+); 2% CO (X) and 5% CO (#).

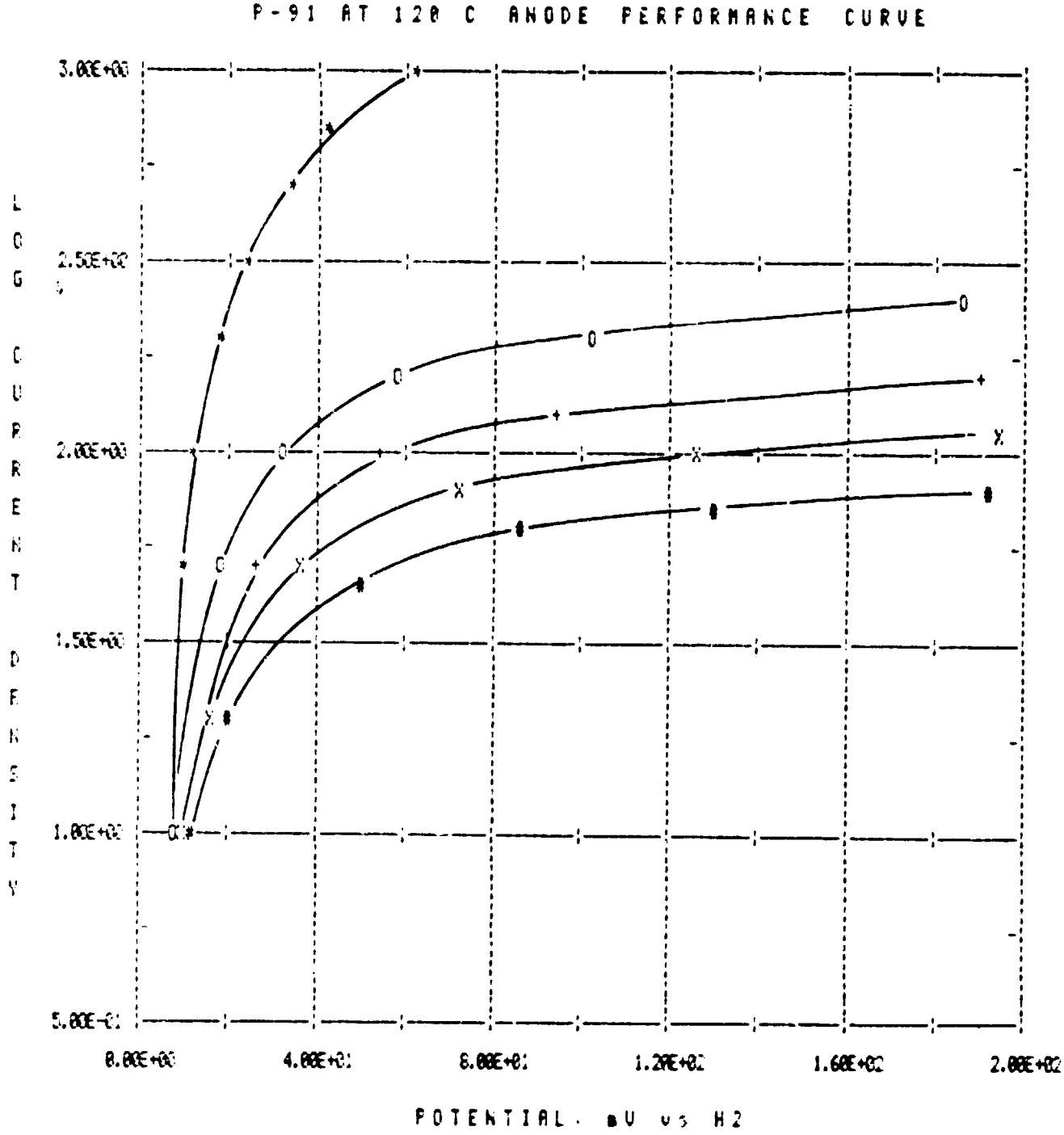

FIGURE 12.

Electrode P-91 at 120°C. 10 w/o Pt on Vulcan XC-72R, 0.5 mg Pt/cm^2 electrode. 100% H_3PO_4. All data corrected for iR. Gas mixtures 75% H_2, balance N_2 with 0% CO (*); 0.5% CO (0); 1% CO (+); 2% CO (X) and 5% CO (#).

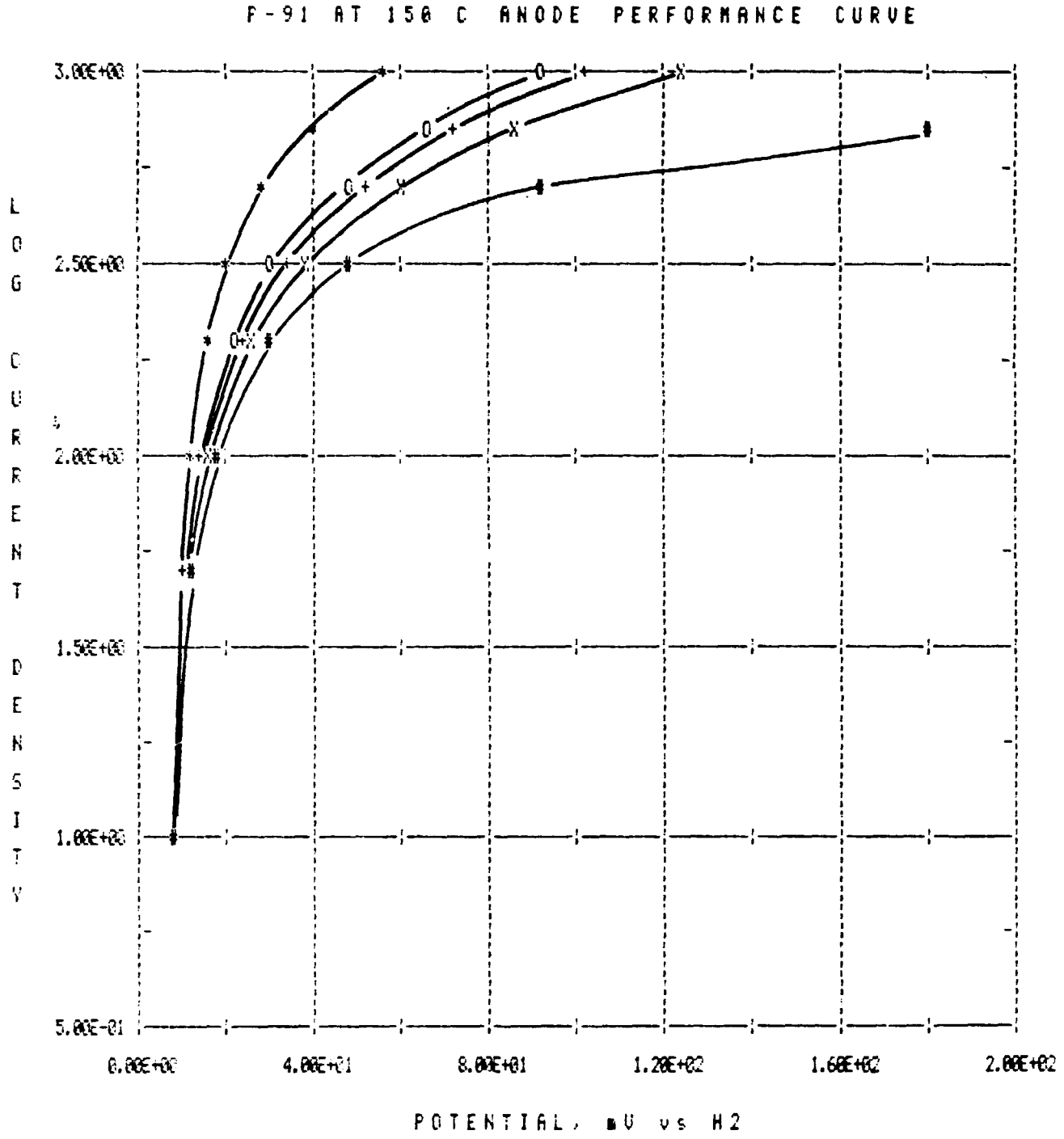

FIGURE 13.

Electrode P-91 at 150°C. 10 w/o Pt on Vulcan XC-72R, 0.5 mg Pt/cm^2 electrode. 100% H_3PO_4. All data corrected for iR. Gas mixtures 75% H_2, balance N_2 with 0% CO (*); 0.5% CO (0); 1% CO (+); 2% CO (X) and 5% CO (#).

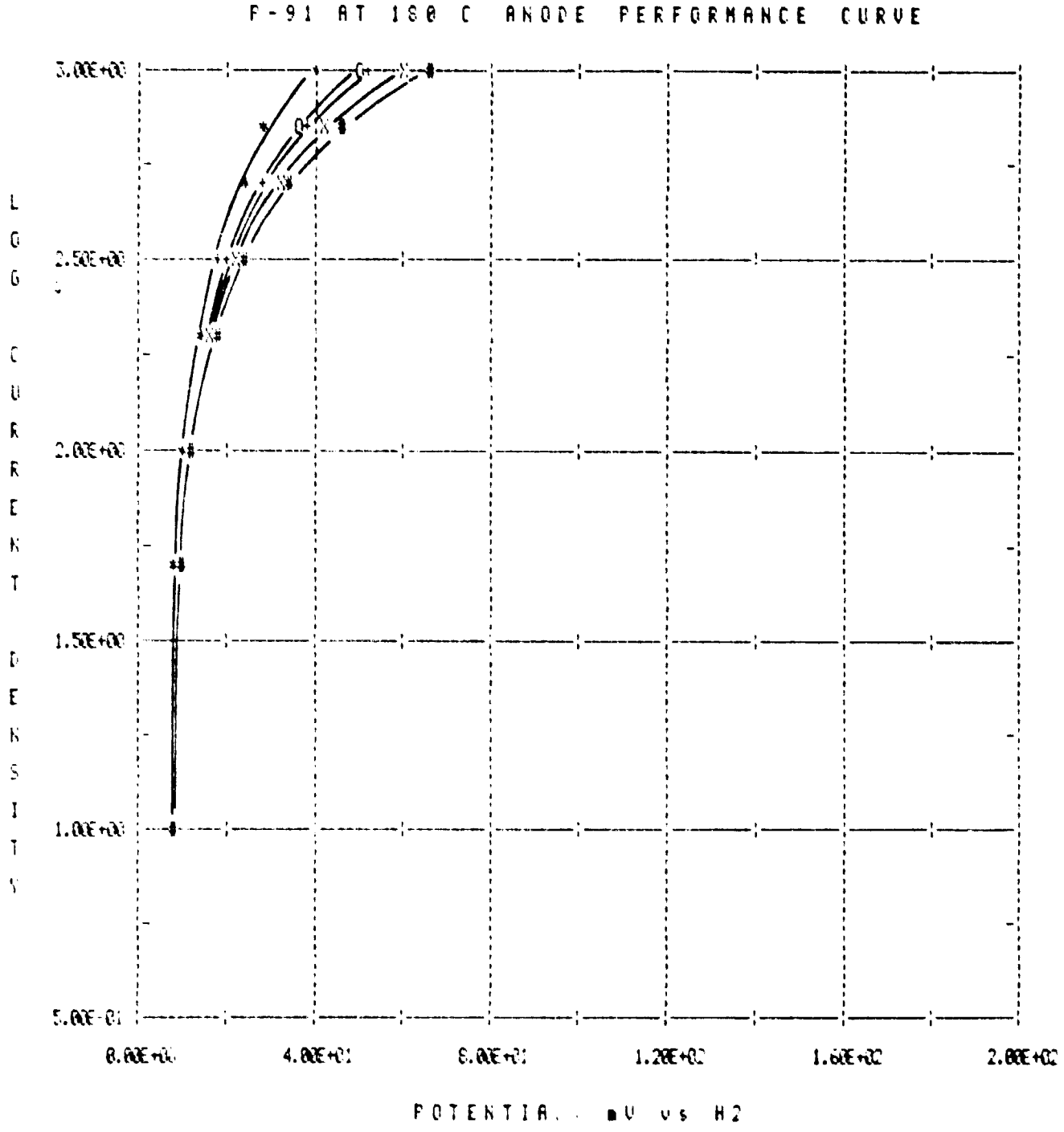

FIGURE 14.

Electrode P-91 at 180°C. 10 w/o Pt on Vulcan XC-72R, 0.5 mg Pt/cm^2 electrode. 100% H_3PO_4. All data corrected for iR. Gas mixtures 75% H_2, balance N_2 with 0% CO (*); 0.5% CO (0); 1% CO (+); 2% CO (X) and 5% CO (#).

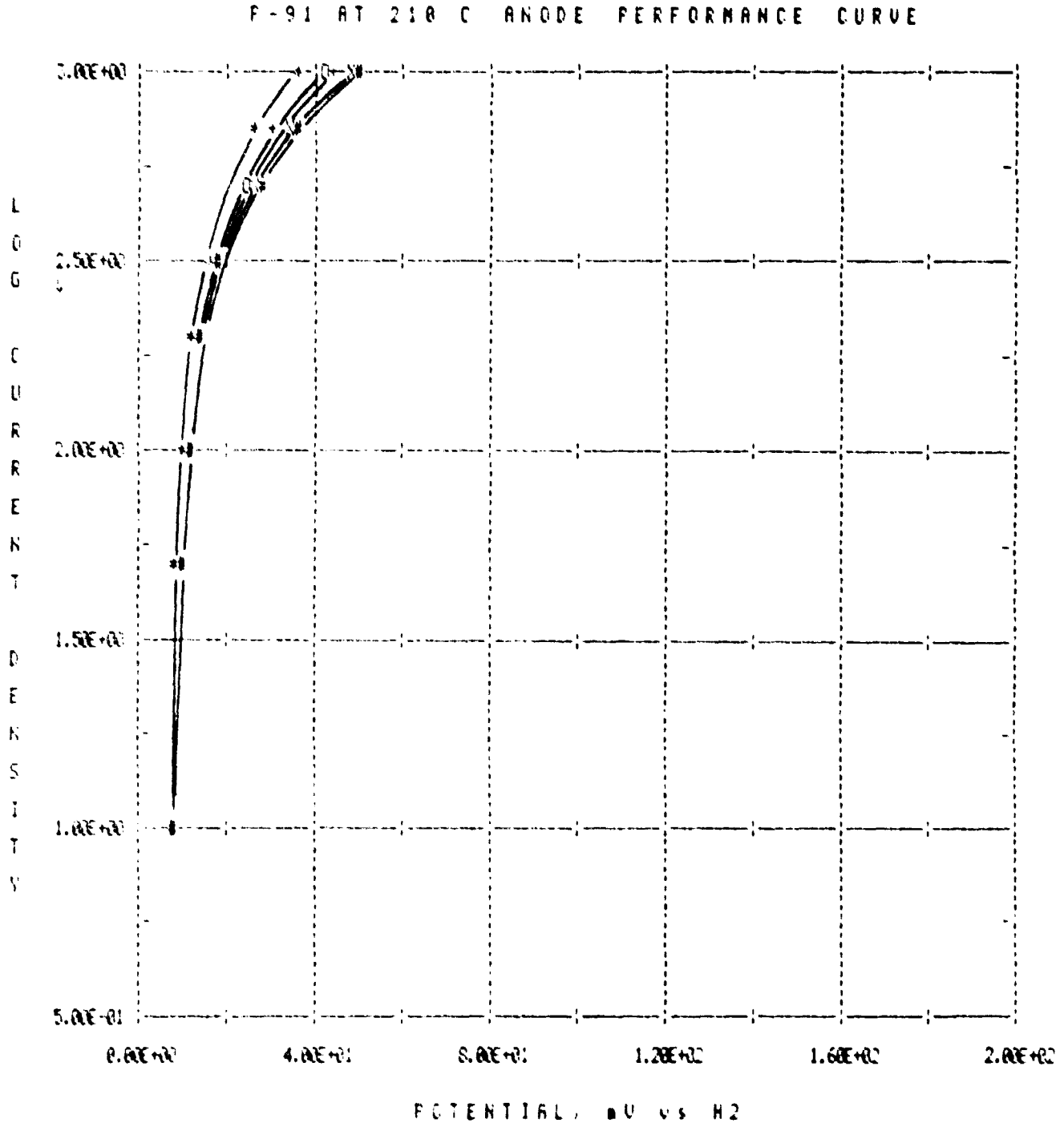

FIGURE 15.

Electrode P-91 at 210°C. 10 w/o Pt on Vulcan XC-72R, 0.5 mg Pt/cm^2 electrode. 100% H_3PO_4. All data corrected for iR. Gas mixtures 75% H_2, balance N_2 with 0% CO (*); 0.5% CO (0); 1% CO (+); 2% CO (X) and 5% CO (#).

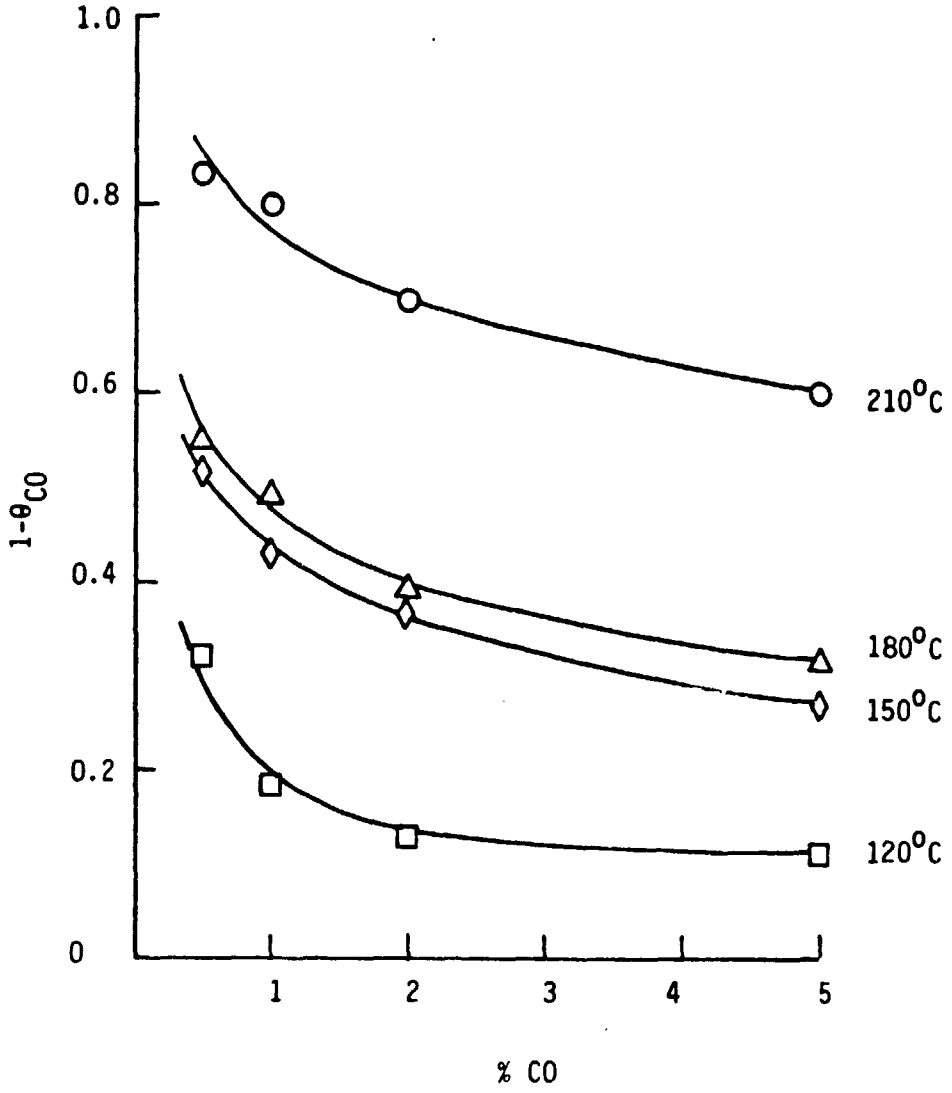

Figure 16.

Electrode P-116. Apparent available surface areas on platinum as a function of temperature and carbon monoxide levels.

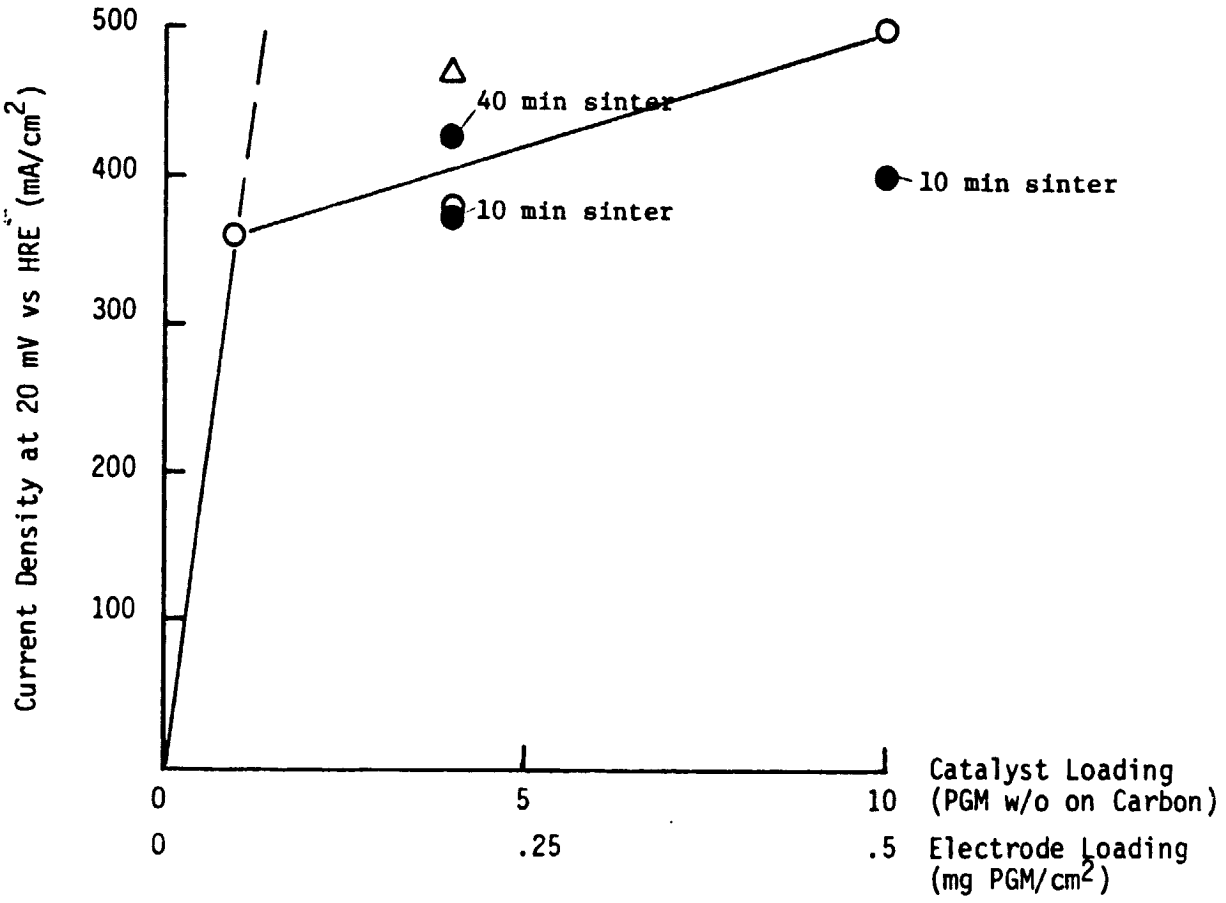

Figure 17.

Hydrogen oxidation reaction rates on platinum supported on Vulcan XC-72R (O) and on platinum-palladium supported on Consel I (Δ). Gas mixture 75% hydrogen; balance nitrogen. 210°C, 100% phosphoric acid. Platinum supported on Consel I (●).

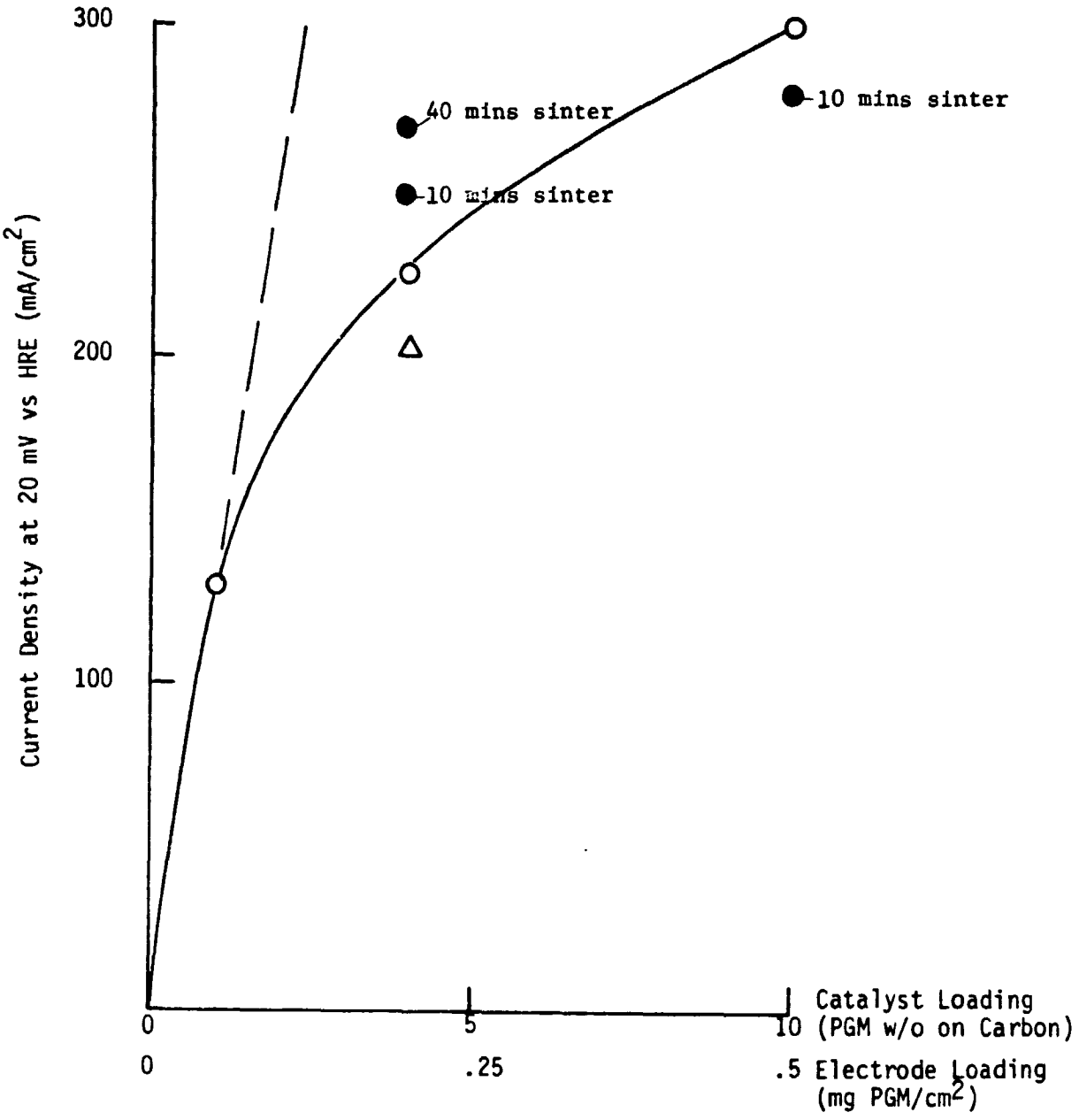

Figure 18.

Hydrogen oxidation reaction rates on platinum supported on Vulcan XC-72R (O) and on platinum-palladium supported on Consel I (Δ). Gas mixture 75% hydrogen; 1% CO; balance nitrogen. 180°C, 100% phosphoric acid. Platinum supported on Consel I (●).

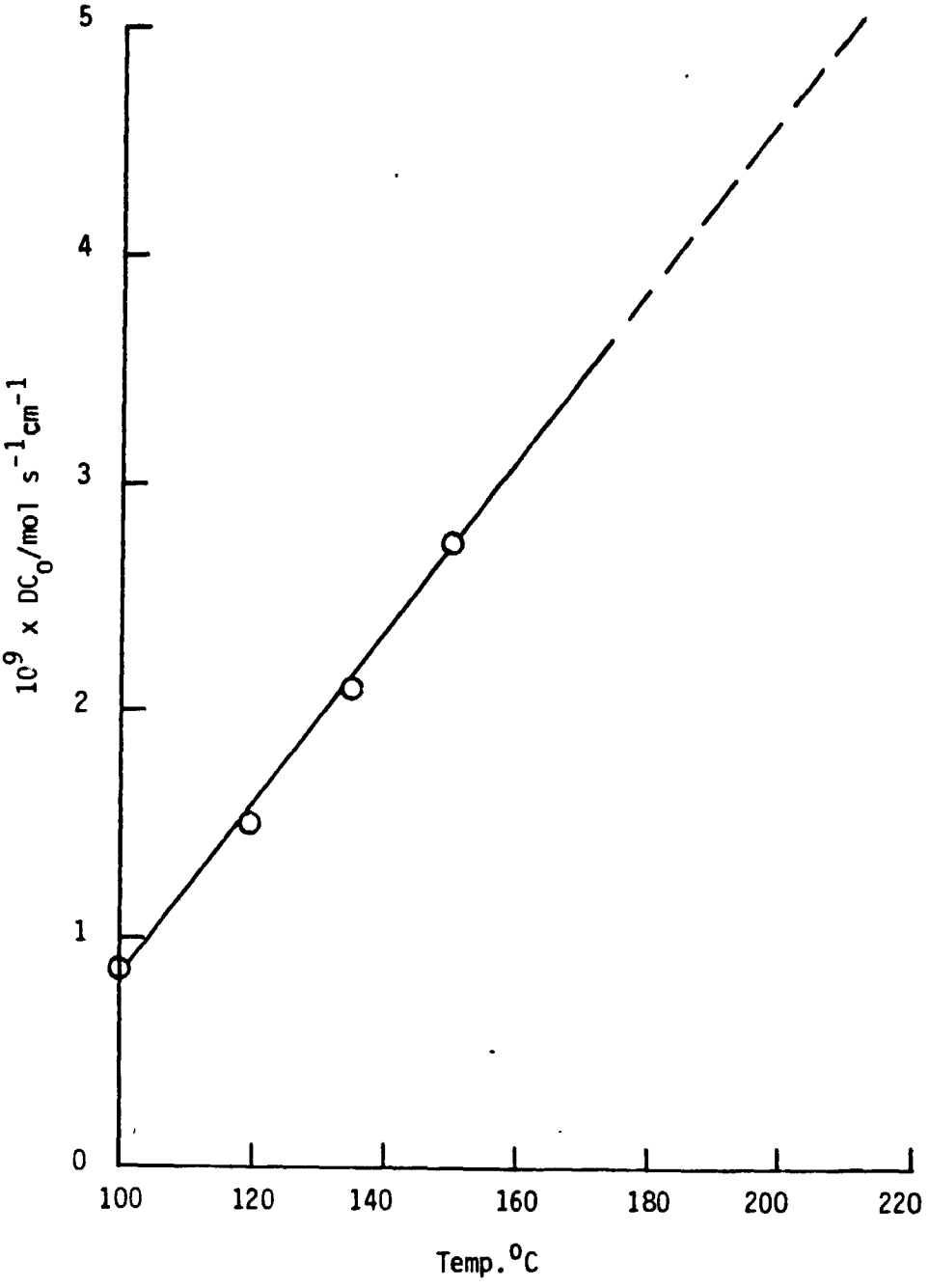

Figure 19.

Solubility-Diffusivity product of oxygen in 100% phosphoric acid. Data extrapolated from Figure 2 of K. Klinedinst, J. A. S. Bett, J. MacDonald, and P. Stonehart, Journal of Electroanalytical Chemistry, 57 (1974) p. 285.

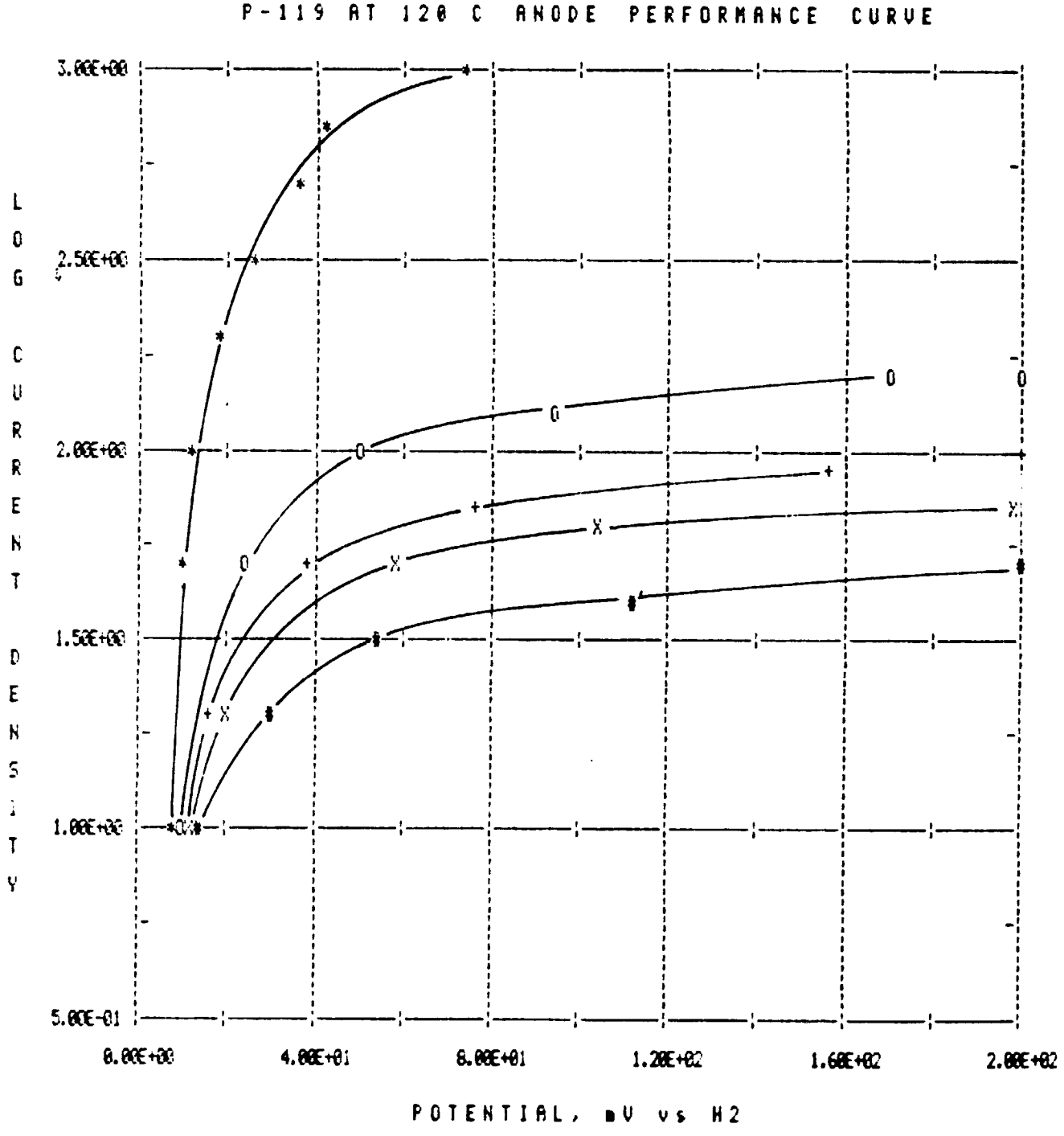

Figure 20.

Electrode P-119 at 120°C. 4 w/o Pt on Consel I, 0.2 mg Pt/cm^2 electrode. 30% PTFE sintered at 315°C for 10 minutes. All data corrected for iR. Gas mixtures 75% H_2, balance N_2 with 0% CO (*); 0.5% CO (0); 1% CO (+); 2% CO (X) and 5% CO (#).

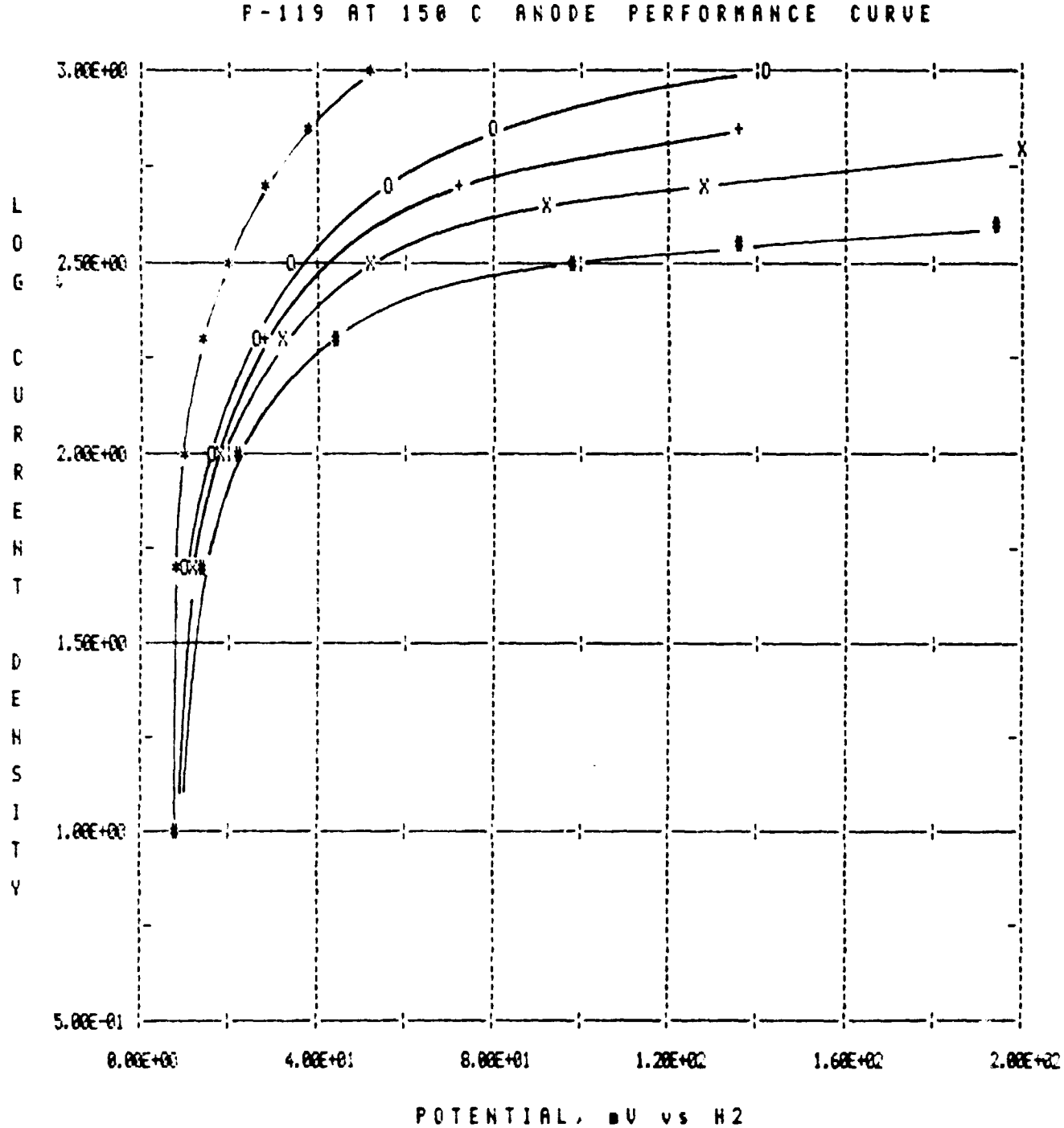

Figure 21.
Electrode P-119 at 150°C. 4 w/o Pt on Consel I, 0.2 mg Pt/cm^2 electrode. 30% PTFE sintered at 315°C for 10 minutes. All data corrected for iR. Gas mixtures 75% H_2, balance N_2 with 0% CO (*); 0.5% CO (0); 1% CO (+); 2% CO (X) and 5% CO (#).

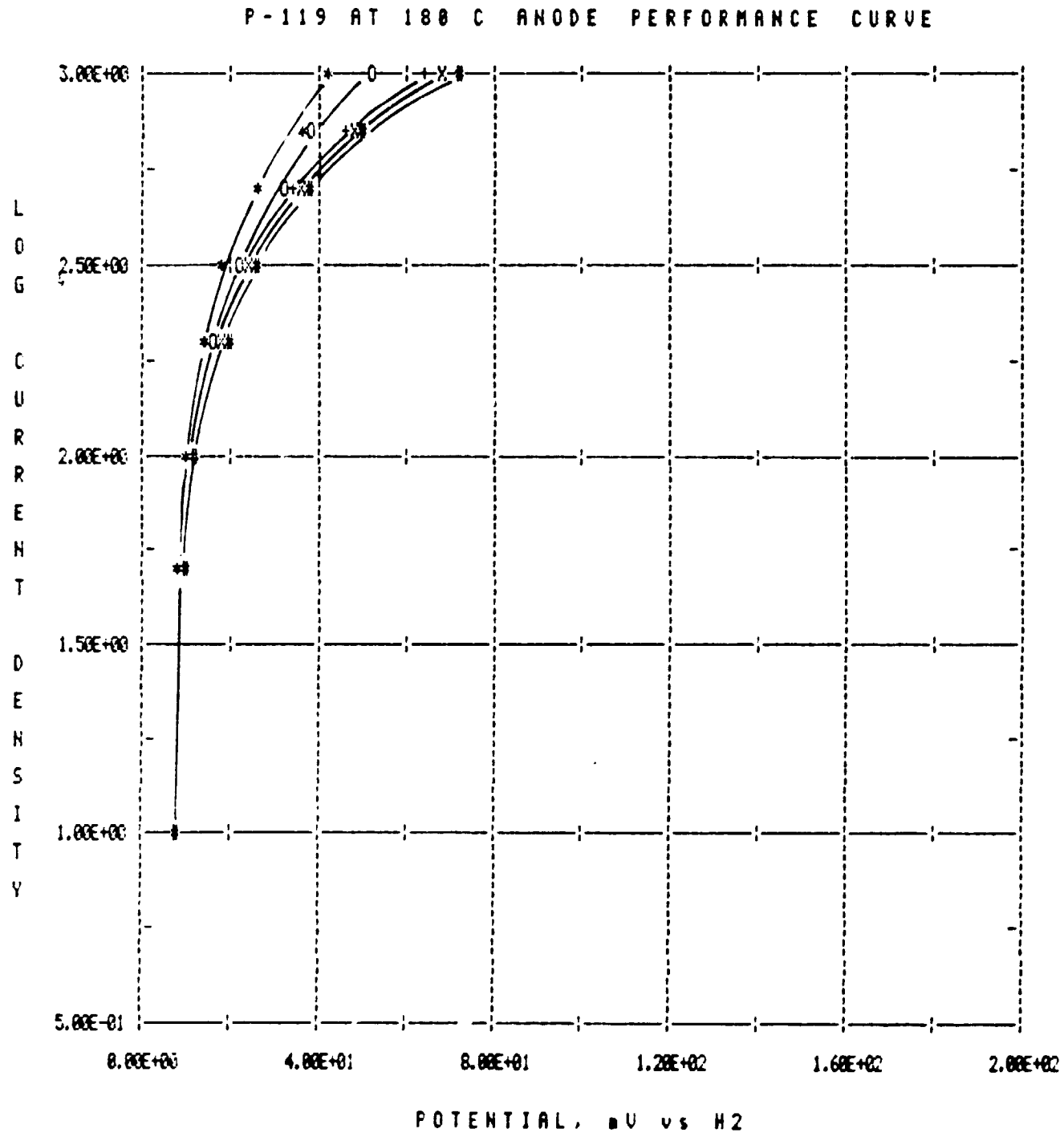

Figure 22.

Electrode P-119 at 180°C. 4 w/o Pt on Consel I, 0.2 mg Pt/cm^2 electrode. 30% PTFE sintered at 315°C for 10 minutes. All data corrected for iR. Gas mixtures 75% H_2, balance N_2 with 0% CO (*); 0.5% CO (0); 1% CO (+); 2% CO (X) and 5% CO (#).

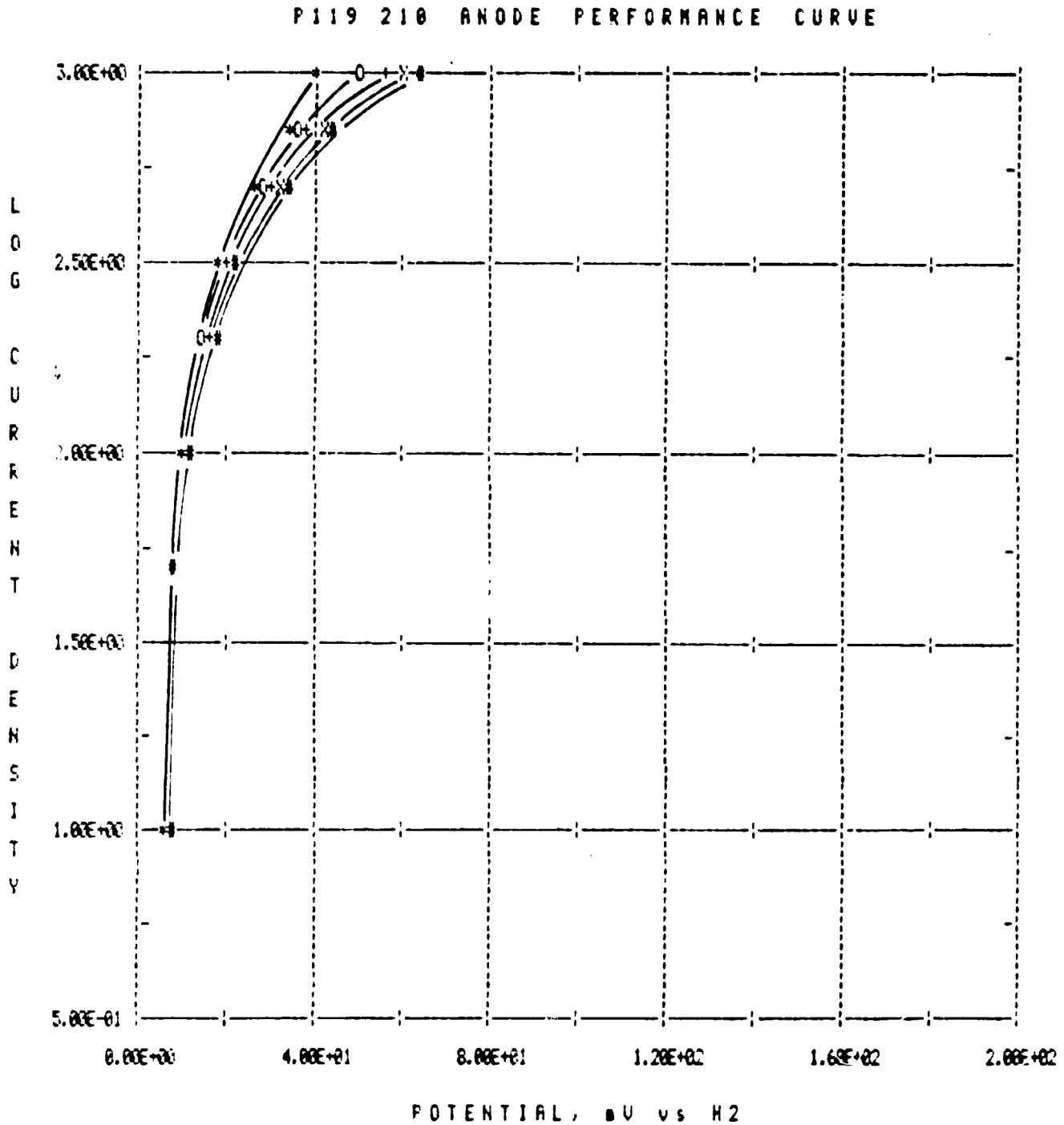

Figure 23.
Electrode P-119 at 210°C. 4 w/o Pt on Consel I, 0.2 mg Pt/cm^2 electrode. 30% PTFE sintered at 315°C for 10 minutes. All data corrected for iR. Gas mixtures 75% H_2, balance N_2 with 0% CO (*); 0.5% CO (0); 1% CO (+); 2% CO (X) and 5% CO (#).

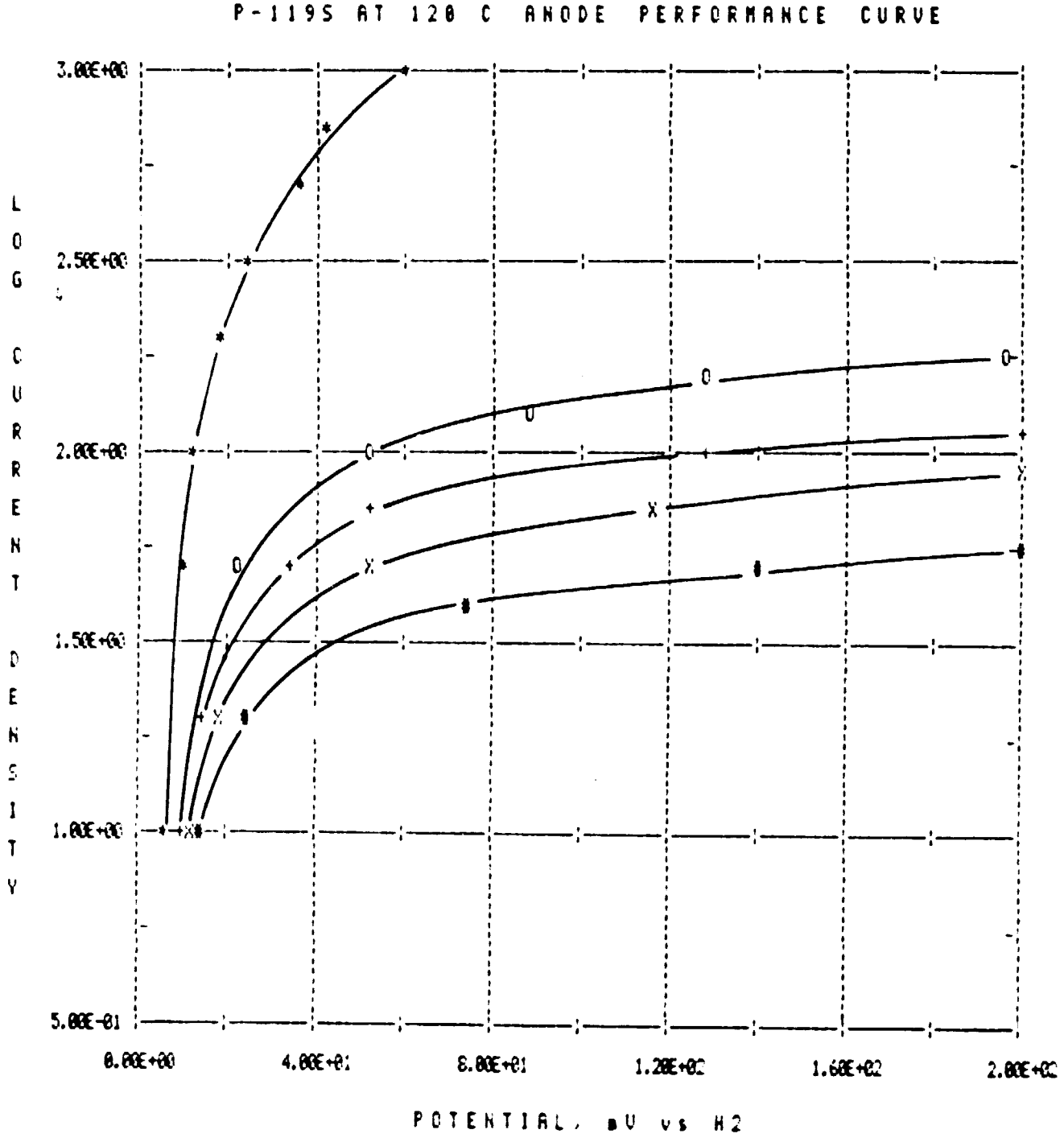

Figure 24.
Electrode P-119S at 120°C. 4 w/o Pt on Consel I, 0.2 mg Pt/cm^2 electrode. 30% PTFE sintered at 315°C for 40 minutes. All data corrected for iR. Gas mixtures 75% H_2, balance N_2 with 0% CO (*); 0.5% CO (0); 1% CO (+); 2% CO (X) and 5% CO (#).

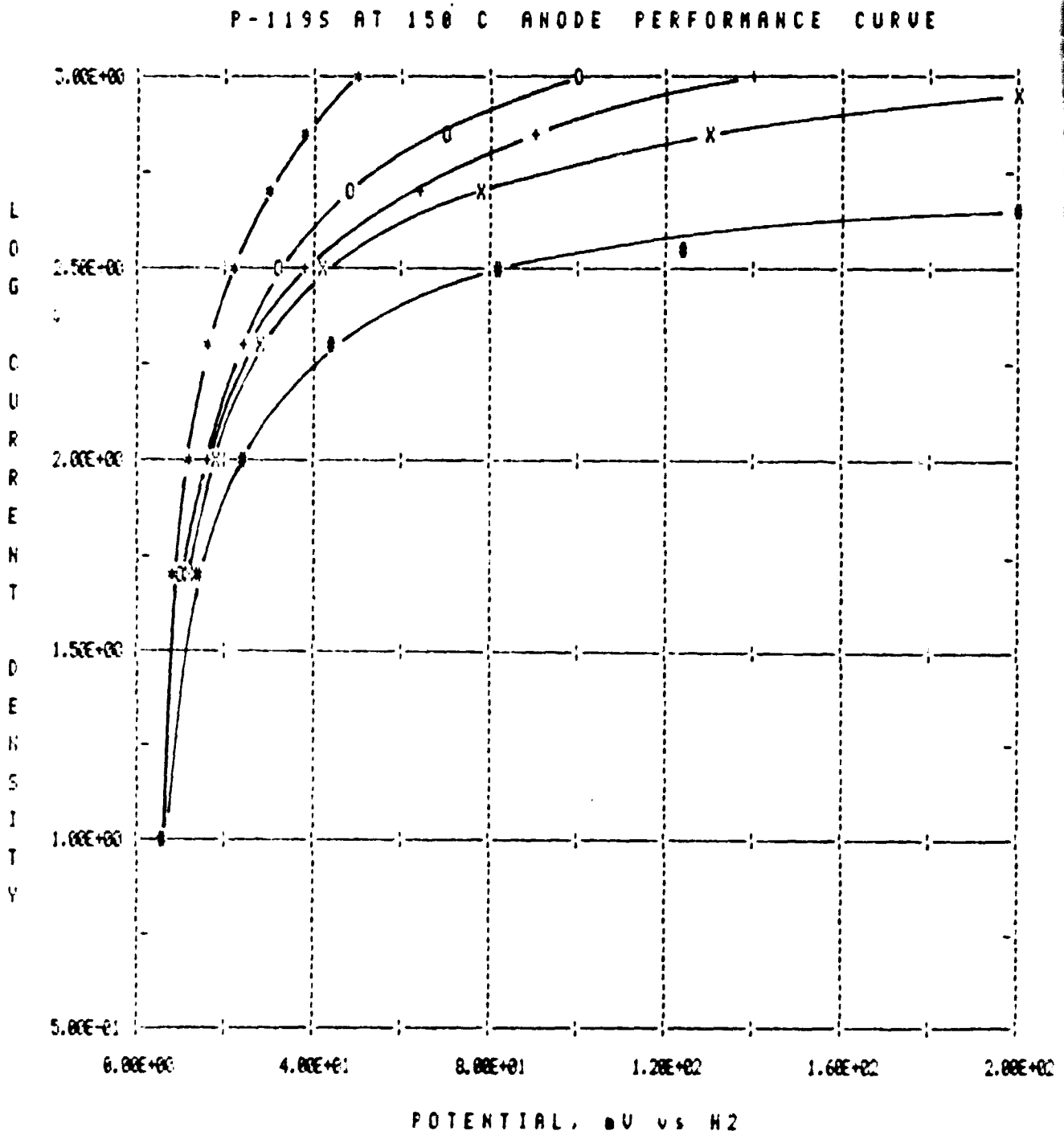

Figure 25.

Electrode P-119S at 150°C. 4 w/o Pt on Consel I, 0.2 mg Pt/cm^2 electrode. 30% PTFE sintered at 315°C for 40 minutes. All data corrected for iR. Gas mixtures 75% H_2, balance N_2 with 0% CO (*); 0.5% CO (0); 1% CO (+); 2% CO (X) and 5% CO (#).

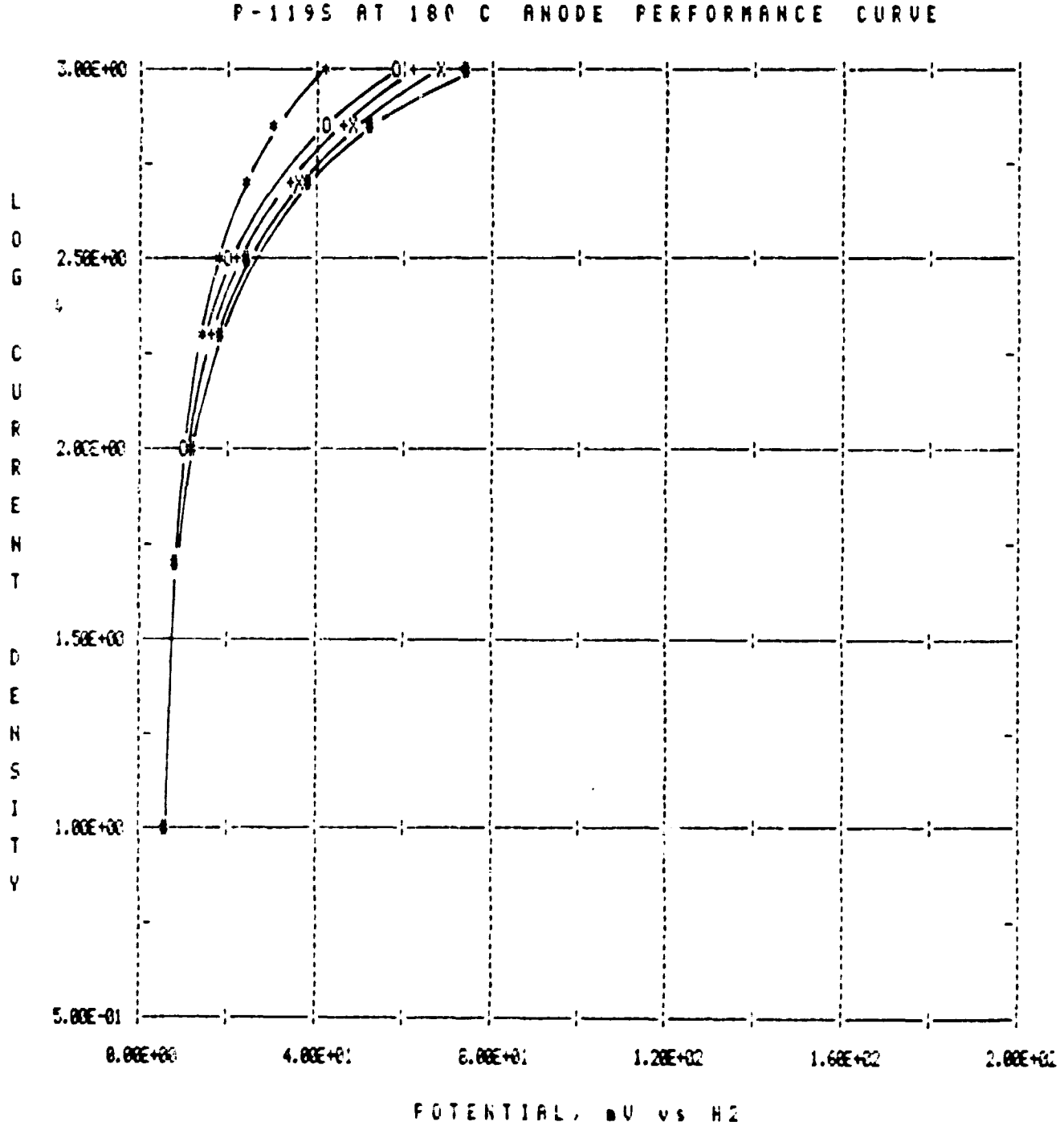

Figure 26.

Electrode P-119S at 180°C. 4 w/o Pt on Vulcan XC-72, 0.2 mg Pt/cm^2 electrode. 30% PTFE sintered at 315°C for 40 minutes. All data corrected for iR. Gas mixtures 75% H_2, balance N_2 with 0% CO (*); 0.5% CO (O); 1% CO (+); 2% CO (X) and 5% CO (#).

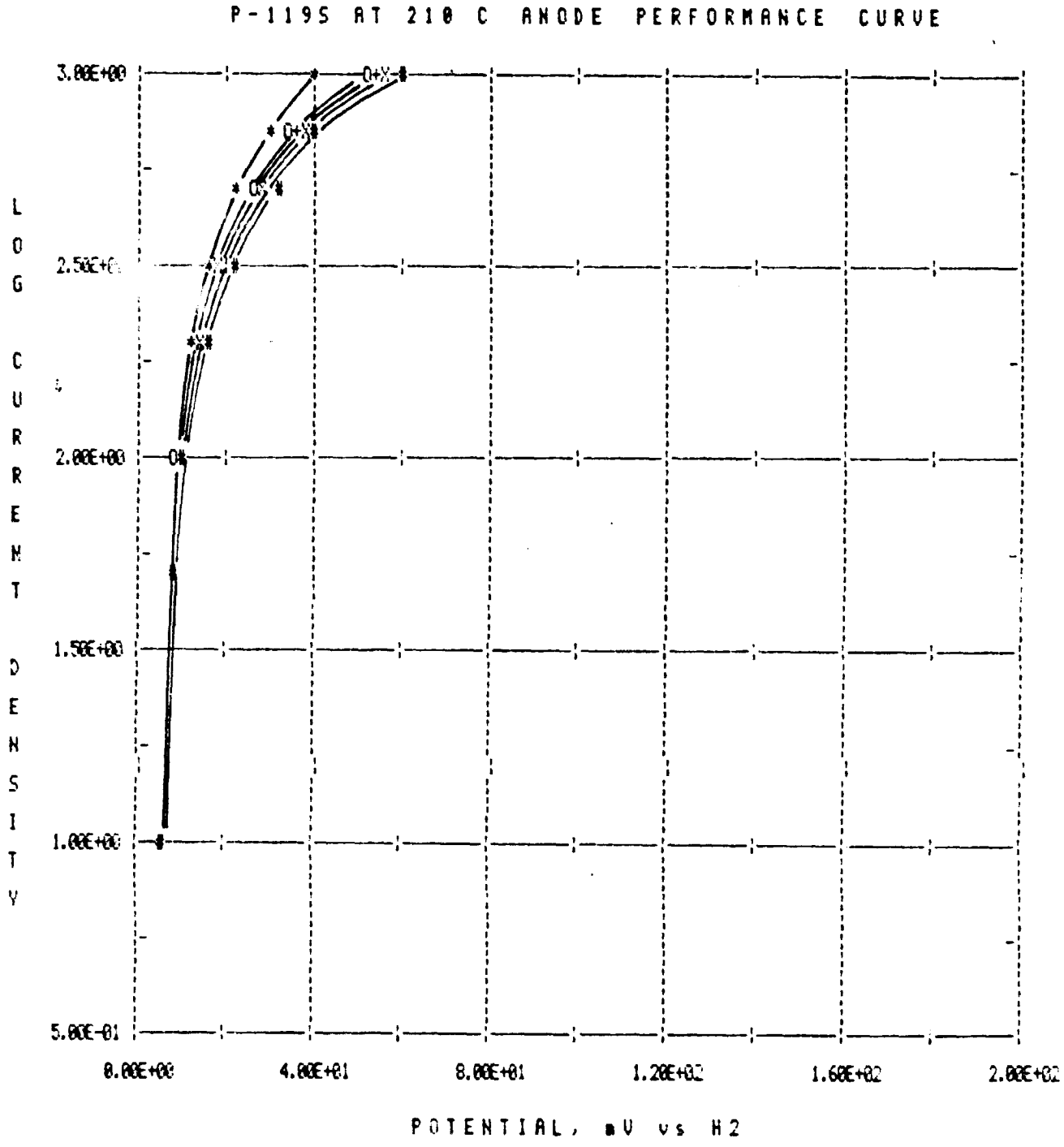

Figure 27.

Electrode P-119S at 210°C. 4 w/o Pt on Consel I, 0.2 mg Pt/cm^2 electrode. 30% PTFE sintered at 315°C for 40 minutes. All data corrected for iR. Gas mixtures 75% H_2, balance N_2 with 0% CO (*); 0 5% CO (0); 1% CO (+); 2% CO (X) and 5% CO (#).

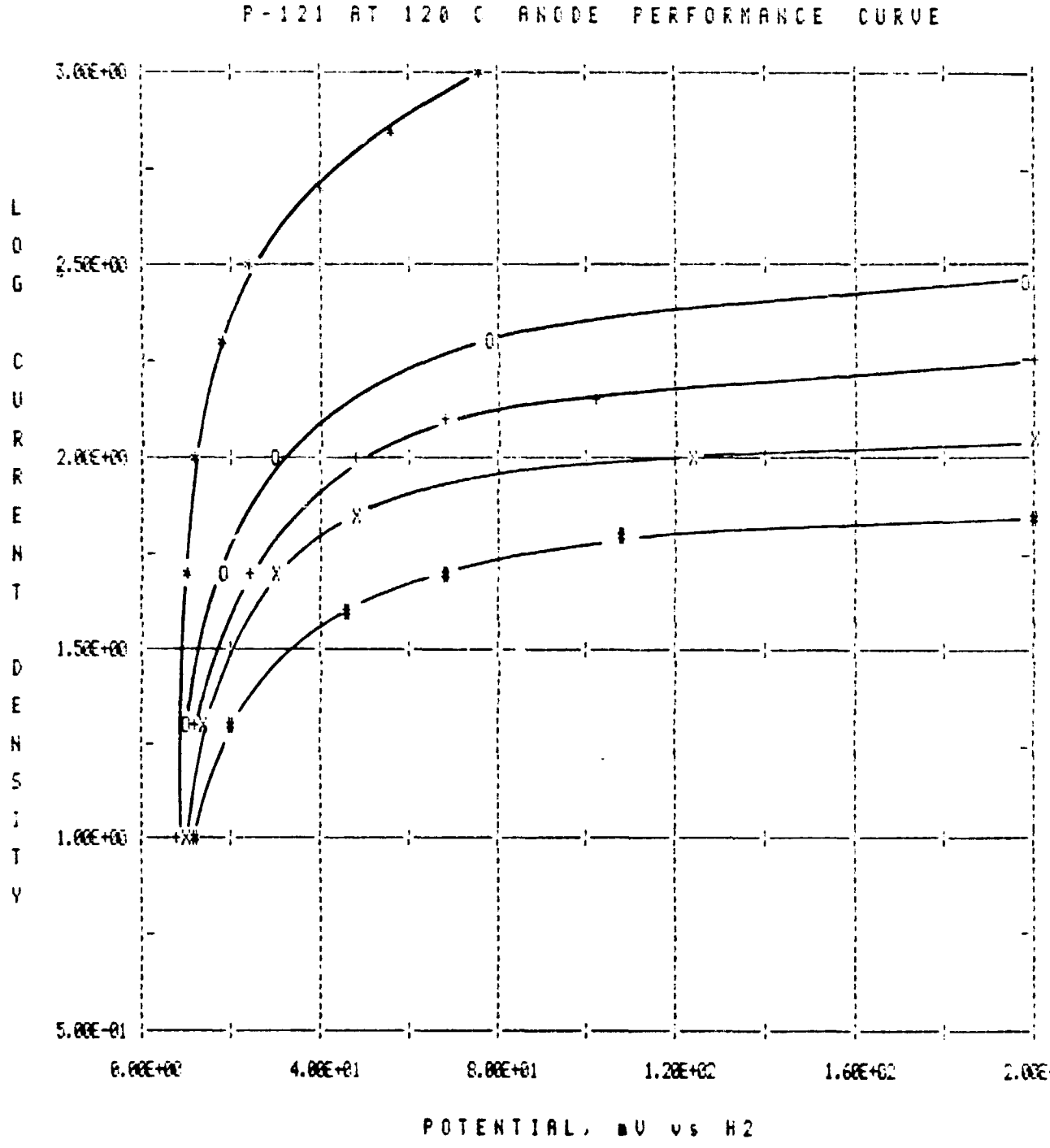

Figure 28.

Electrode P-121 at 120°C. 10 w/o Pt on Consel I, 0.5 mg Pt/cm^2 electrode. 30% PTFE sintered at 315°C for 10 minutes. All data corrected for iR. Gas mixtures 75% H_2, balance N_2 with 0% CO (*); 0.5% CO (0); 1% CO (+); 2% CO (X) and 5% CO (#).

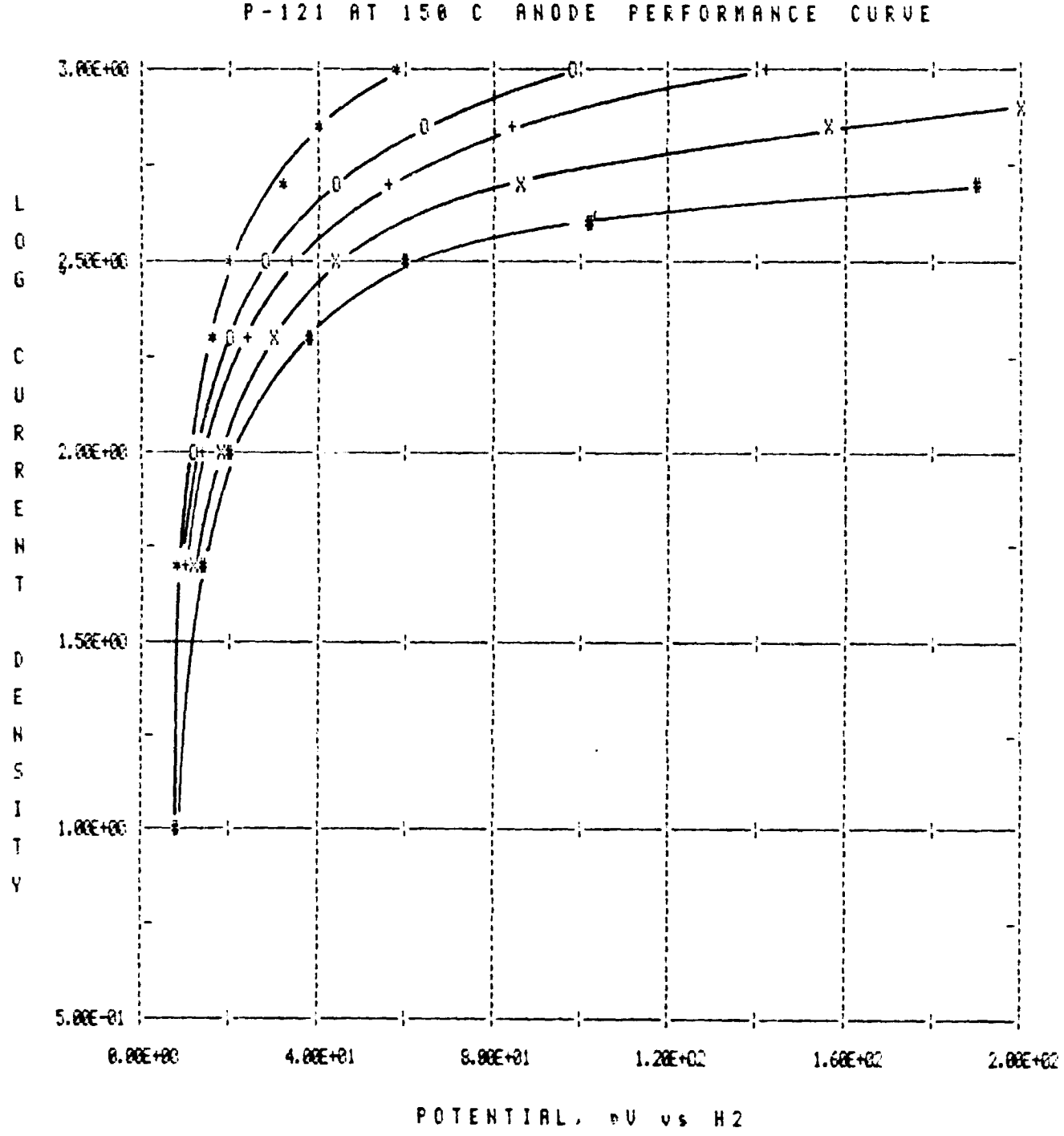

Figure 29.

Electrode P-121 at 150°C. 10 w/o Pt on Consel I, 0.5 mg Pt/cm^2 electrode. 30% PTFE sintered at 315°C for 10 minutes. All data corrected for iR. Gas mixtures 75% H_2, balance N_2 with 0% CO (*); 0.5% CO (0); 1% CO (+); 2% CO (X) and 5% CO (#).

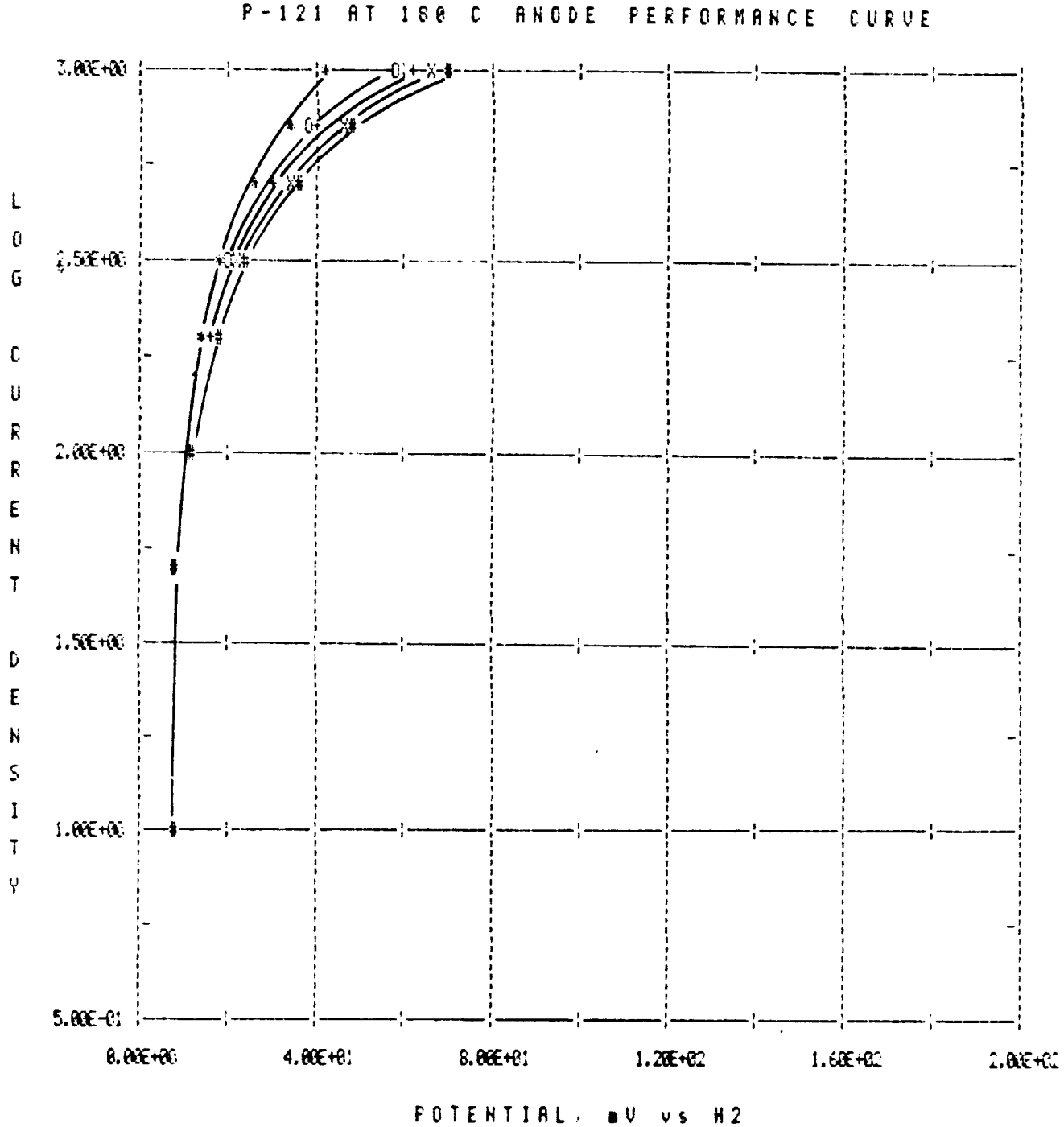

Figure 30.
Electrode P-121 at 180°C. 10 w/o Pt on Consel I, 0.5 mg Pt/cm^2 electrode. 30% PTFE sintered at 315°C for 10 minutes. All data corrected for iR. Gas mixtures 75% H_2, balance N_2 with 0% CO (*); 0.5% CO (0); 1% CO (+); 2% CO (X) and 5% CO (#).

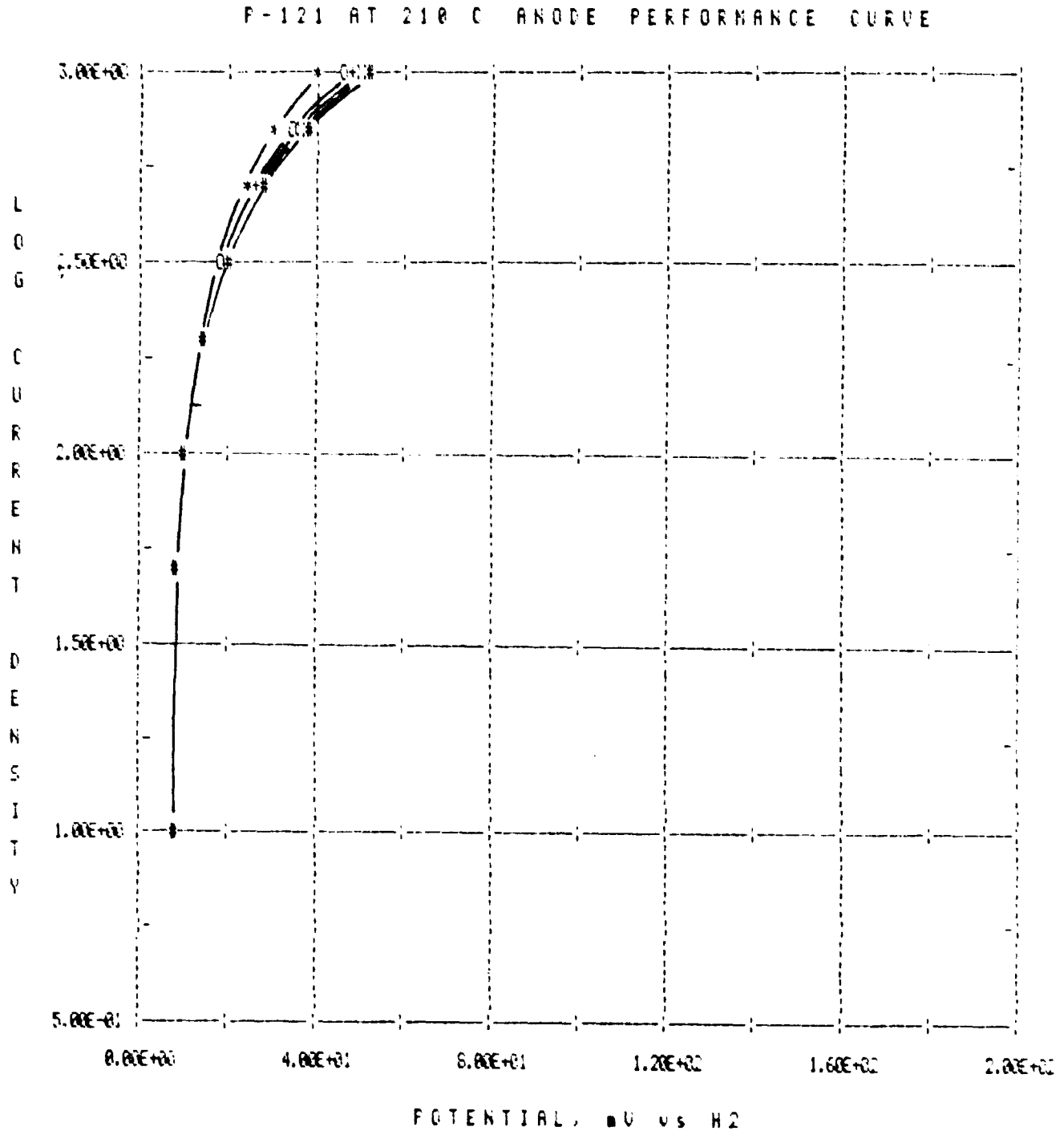

Figure 31.
Electrode P-121 at 210°C. 10 w/o Pt on Consel I, 0.5 mg Pt/cm^2 electrode. 30% PTFE sintered at 315°C for 10 minutes. All data corrected for iR. Gas mixtures 75% H_2, balance N_2 with 0% CO (*); 0.5% CO (0); 1% CO (+); 2% CO (X) and 5% CO (#).